The Thesis Committee for Anthony Brandon McGlown
Certifies that this is the approved version of the following thesis:

Transitional flow deposits in submarine lobe strata: the Cretaceous Point Loma Formation, San Diego, California

APPROVED BY
SUPERVISING COMMITTEE:

Supervisor:

David Mohrig

Peter Flemings

Julian Clark

Transitional flow deposits in submarine lobe strata: the Cretaceous Point Loma Formation, San Diego, California

by

Anthony Brandon McGlown, B.S. Geo.

Thesis

Presented to the Faculty of the Graduate School of

The University of Texas at Austin

in Partial Fulfillment

of the Requirements

for the Degree of

Master of Science in Geological Sciences

The University of Texas at Austin

May 2015

Acknowledgements

I would like to express my sincere thanks to David Mohrig for his guidance, enthusiasm, and time. I would also like to thank Peter Flemings and Julian Clark for their advice and reviews during the writing of this thesis. I am grateful to Jim Buttles, Mauricio Perillo, and fellow students in the Mohrig research group for all of the feedback and discussions that have helped me develop my research. Thanks to David Brown for his help with field work in San Diego. I would also like to acknowledge financial support provided by the Jackson School of Geosciences, ConocoPhillips, and Statoil. Finally, I want to thank my wife Kelley for her love, patience, and support over the past two years.

Abstract

Transitional flow deposits in submarine lobe strata: the Cretaceous Point Loma Formation, San Diego, California

Anthony Brandon McGlown, M.S. Geo. Sci.

The University of Texas at Austin, 2015

Supervisor: David Mohrig

Transitional flow deposits (TFDs) include a spectrum of subaqueous sediment-gravity flow deposits that do not fit conventional models for turbidites and debrites. Examples of TFDs are common in submarine lobe strata of the Cretaceous Point Loma Formation in San Diego, California. The cross-flow orientation and exceptional quality of this sea cliff exposure presents a unique opportunity to document axis-to-margin variability within individual beds. TFDs in the Point Loma Formation are typically composed of a lower interval of structureless sandstone that is overlain by meso- to micro-banded sandstone with high mud content. This upward transition from sandstone with lower mud content to overlying mud-rich sandstone is characteristic of TFDs worldwide. Cross-flow exposure reveals a corresponding change in geometry: a lenticular 'core' of structureless sandstone is overlain by an extensive, mud-rich 'drape' of banded sandstone. This internal shift in both composition and geometry is interpreted to reflect deposition from two distinct stages of transitional flows. Initial deposition of coarser sand

was spatially restricted while flows were energetic and able to efficiently segregate particles of different size. Following this initial stage of deposition and energy loss, flows deposited muddy sand over a wider area; this transition is interpreted to reflect a change in current behavior where reduced flow velocity coincided with decreased mixing and poor segregation of suspended sand and mud fractions during deposition.

The organization of TFDs within the outcrop varies with scale. Multiple TFDs stack to form lobe elements with minimal lateral offset between bed axes. As a result, both individual beds and lobe elements show relatively simple transitions from sand-prone axes to mud-rich margins. Compensational stacking of lobe elements introduces additional complexity at larger scales, where vertical alternation between sandy and mud-rich units reflects significant lateral shifts in position (ca. 500 m to 1 km) between the axes of successive lobe elements. Bed thickness frequency analysis shows how differences between distributions of vertically measured thicknesses relate to the spatial variability in outcrop. Developing a better understanding of these relationships is critical for applications in both industry and academia in which workers are frequently limited to using one-dimensional data sets.

Table of Contents

List of Tables

List of Figures

1: Introduction

Transport of sediment to terminal deep-marine settings is commonly attributed to turbidity currents and debris flows (Carter, 1975; Middleton & Hampton, 1976; Lowe, 1979, 1982; Nardin et al., 1979). More recently, widespread recognition of anomalous deposits in submarine fan successions has illustrated that turbidites and debrites represent end members of a much broader depositional spectrum (Haughton et al., 2003; Talling et al., 2004; Amy and Talling, 2006; Haughton et al., 2009). Extensively studied examples with interpreted turbidite and debrite components are referred to as "hybrid" event beds or "linked" turbidite-debrite beds (Haughton et al., 2003; Talling et al., 2004) and are interpreted to record deposition from currents that transition from turbidity current to cohesive debris flow. A broad range of deposits in both modern and ancient turbidite systems display features that are not easily attributed to deposition from idealized, fully turbulent turbidity currents or high-strength debris flows (Lowe and Guy, 2000; Kane and Ponten, 2013). Interpretation of such transitional flow deposits (TFDs) can be particularly problematic, as the wide variety of deposit features that can result from transitional flows are poorly understood.

The ability to document the stratigraphic organization of TFDs and to describe lateral variability within individual beds can potentially add a wealth of information toward interpreting flow behavior. Drill core and field studies in which individual beds have been mapped over large distances provide significant insight into spatial changes in

flow behavior (Amy and Talling, 2006; Ito, 2008; Hodgson, 2009; Talling et al., 2012a; Stevenson et al., 2013). Relatively few studies have documented cross-flow variability within individual TFDs and TFD-dominated stratigraphy (Amy and Talling, 2006; Stammer, 2014). Cross-flow variability in flow behavior occurs over much smaller spatial scales and stands a better chance of being preserved in continuous outcrop exposure. Unfortunately, outcrop examples that are both suitably well-exposed and laterally extensive are uncommon.

Outcrop of the Cretaceous Point Loma Formation in San Diego, California, offers an exceptional combination of well-exposed submarine lobe strata and high lateral continuity. In addition, most of the outcrop is oriented perpendicular to paleocurrent (Yeo, 1982; Fleming, 2010), providing an extensive cross-flow view of individual beds and larger-scale lobe architecture. Recent studies on this outcrop have documented examples of argillaceous deposits interpreted as TFDs (Fleming, 2010; Stammer, 2014). This contribution utilizes the exceptional exposure of submarine lobe strata in the Point Loma Formation to address a number of key questions:

Question 1: What are the characteristics of TFDs in the Point Loma Formation? Can we learn anything new using information about cross-flow variability within beds?

Primary sedimentary features record the near-bed dynamics of depositional currents, and facies models use the assemblages of features within deposits to interpret the overall behavior and evolution of parent flows (Bouma, 1962; Lowe, 1982; Pickering et al., 1986; Mutti, 1992; Haughton et al., 2009). There are, however, major limitations to

how much can be learned about a given flow from its deposit alone. Periods of sediment bypass or erosion, for example, leave no depositional record behind. In addition, different types of experimental flows have been observed to produce visually similar deposits; examples include fine planar-laminated sands deposited from flows with relatively high near-bed sediment concentrations (Kuenen, 1966; Bannerjee, 1977; Arnott & Hand, 1989; Leclair & Arnott, 2005; Sumner et al., 2008) and parallel laminated sands formed by the migration of low-amplitude bedwaves beneath dilute flows (Best & Bridge, 1992).

Particularly relevant to this study are structureless sands, for which natural examples have been variably attributed to deposition from turbidity currents (Lowe, 1982; Kneller and Branney, 1995), "sandy" debris flows (Shanmugam, 1996), and settling of coarser sand fractions from mud-rich, weakly to moderately cohesive debris flows (Talling et al., 2012a). With such a variety of potential depositional mechanisms for these deposits, the reliability of straightforward interpretations—particularly those from limited exposure in outcrop or drill core—remains questionable. Such interpretations might be improved by the incorporating observations about lateral variability within deposits.

Question 2: What is the spatial distribution of TFDs within distal lobe architecture? What are the processes controlling this distribution at different spatial scales?

Studies using subsurface well data and long-distance outcrop correlations suggest that hybrid beds and TFDs are particularly common in the distal and lateral margin portions of submarine fan systems (Haughton et al., 2003; Talling et al., 2004; Amy and

Talling, 2006; Ito, 2008; Hodgson, 2009; Kane and Ponten, 2013). Such distal fan settings are characterized by terminal lobes at the down-flow ends of channel-levee systems. Outcrop examples of lobe strata have been shown to have scale-dependent internal architectures (Straub and Pyles, 2012). This type of architectural framework can potentially be used to tie the spatial distribution of TFDs to specific processes at different scales. In addition, an understanding of how TFDs are distributed at different scales could be used to help model heterogeneity within analogous subsurface reservoirs.

Question 3: Is the frequency distribution of bed thicknesses in TFD-dominated lobe strata different from that present in turbidite successions? Can similarities and/or differences be linked to specific processes? How does cross-flow variability impact bed thickness distributions?

The frequency distribution of bed thicknesses in a vertical stratigraphic section contains information about the spatial arrangement of deposits within a larger stratigraphic volume. This arrangement reflects variability between the currents that deposited each bed, such as differences in flow volume or composition, in addition to lateral shifts in flow trajectory over time. A number of studies have shown that thicknesses within turbidite strata are well described by lognormal distributions (Murray et al., 1996; Talling, 2001; Sylvester, 2007). Talling (2001) and Sylvester (2007) further showed that such distributions can result from the combination of lognormal subpopulations corresponding to either ‘thick-bedded’ or ‘thin-bedded’ turbidites. The primary difference between these two types of turbidites is the presence or absence of

basal structureless sandstone divisions. Bed thicknesses are analyzed in this study to compare thickness frequency distributions for TFDs with those reported for turbidite successions. In addition, the continuous exposure of the Point Loma Formation is used here to describe how lateral variability in lobe strata impacts bed thickness distributions from vertical measured sections.

2: Geologic setting

The Point Loma Formation, originally described by Kennedy and Moore (1971), is the middle unit of the Cretaceous Rosario Group. The Rosario Group was deposited in a forearc basin setting during the subduction of the Farallon Plate under the North American Plate (Atwater, 1970; Nilsen and Abbott, 1979; Yeo, 1984). The Point Loma Formation unconformably overlies alluvial fan strata of the Lusardi Formation (Peterson, 1970) and is overlain by channelized inner-fan sandstones and conglomerates of the Cabrillo Formation (Jones and Peterson, 1973; Nilsen and Abbott, 1981; Yeo, 1982). The Point Loma Formation comprises a succession of interbedded marine sandstones and siltstones that are separated into three units by Sliter (1979) and Yeo (1982). The lower sandstone-dominated unit is exposed at La Jolla Bay, north of the Point Loma Peninsula, is interpreted by Nilsen and Abbott (1981) and Yeo (1982) as a paralic succession deposited in a high-energy shelf environment.

The interval of interest for this study includes the middle and upper units of the Point Loma Formation, which are exposed as sea cliffs along the west side of the Point Loma Peninsula (Fig. 1; Fig 2). The middle and upper units have been previously interpreted as outer-fan and middle-fan submarine lobes, respectively, and the transition between the two is interpreted to record submarine fan progradation (Nilsen and Abbott, 1981; Yeo, 1982). More recently, this interval was interpreted as a distributive channel-lobe system showing overall basinward progradation by Fleming (2010).

The Pleistocene-aged Rose Canyon Fault zone is the major structural feature in the San Diego area and lies to the east of the Point Loma Peninsula (Peterson, 1970; Kennedy, 1975). A related syncline is locally centered along Mission Bay, which separates the outcrop between La Jolla and the Point Loma Peninsula. Exposed strata of the Point Loma Formation are relatively undeformed. Fleming (2010) documented seventy small-scale faults within the exposure on the Point Loma Peninsula, of which only three have vertical offsets greater the height of the outcrop (> 10 m).

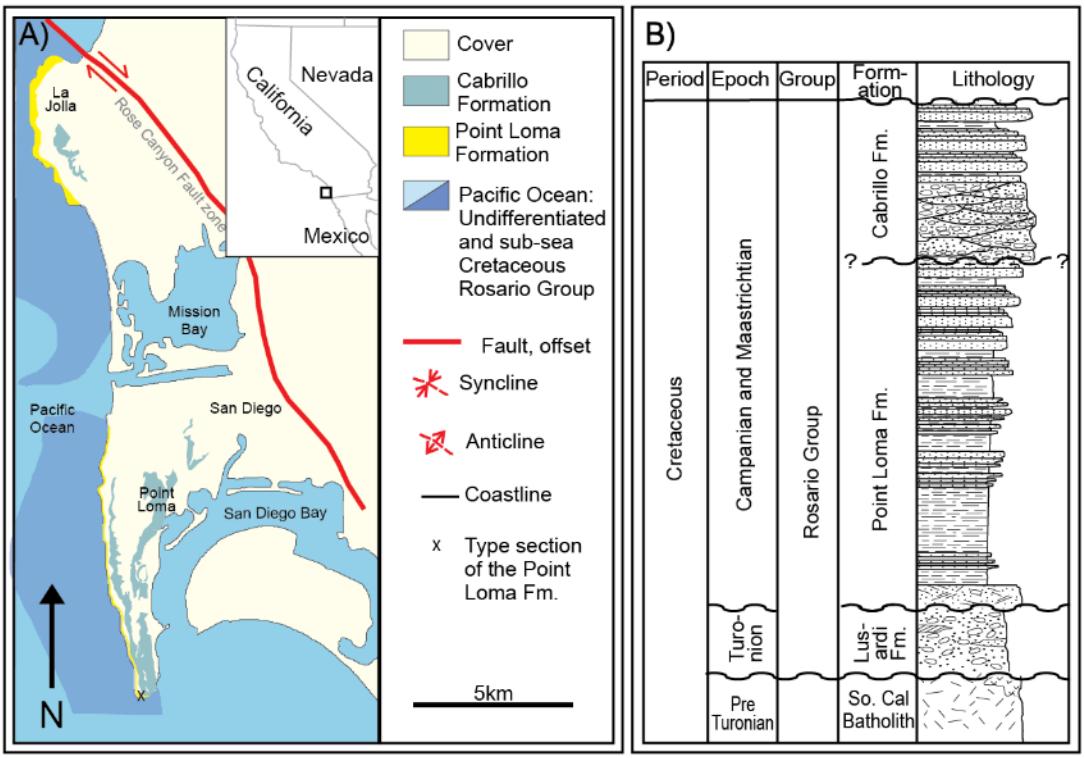

Figure 1. A) Geologic map of the San Diego, California area including the Point Loma Peninsula (map modified from Kennedy and Tan, 2005 and Fleming, 2010). B) Overview of Cretaceous stratigraphy in the San Diego area (modified from Nilsen and Abbott, 1981).

3: Stratigraphic architecture

Fleming (2010) separated the ~7 km lateral exposure and ~90 m stratigraphic thickness of the Point Loma Peninsula into four distinct lobe complexes consisting of 27 lobe elements and four mass transport deposits. A lobe element is defined in depositional-strike view as a meso-scale (>1 m thick and >20 m wide) lithostratigraphic unit with relatively flat lower and upward-convex upper bounding surfaces (Pyles, 2007). The maximum thickness of lobe elements in the Point Loma Formation ranges from 1-4 m (Fleming, 2010). Lobe elements are grouped into lobe complexes that are distinguished by abrupt changes in lithology and lateral shifts in the position of relatively thick and sand-rich axial strata (Fleming, 2010).

The field area for this study is divided into three regions that are bounded by large-offset faults (Fig. 2). The lobe complex interpreted as the most proximal of the exposed lobe strata lies in the northern region (Fig. 3). The north complex consists of lobe elements that are primarily oriented parallel to paleo-depositional dip and comprise coarse to very fine sandstone and interbedded siltstone with frequent bed amalgamation and erosional incision up to 2 m. Lobe strata exposed in the central and southern regions are largely oriented along depositional strike, allowing cross-flow variability within individual beds to be described over tens to hundreds of meters. The central region contains a lower medial to distal lobe complex and an upper medial lobe complex (Fig. 4A, Fig. 4B). Sandstones in the lower central complex range from lower medium to very fine sand. Bed amalgamation is rare and only minor incision is documented (< 30 cm).

The upper central complex contains lower coarse and finer sands with amalgamation in the axes of some lobe elements and incision with < 70 cm relief. The southern region contains one distal lobe complex with a maximum grain size of upper fine sand (Fig. 5). Sandstone amalgamation was not observed in the south complex and erosion surfaces are rare with incision depths < 10 cm.

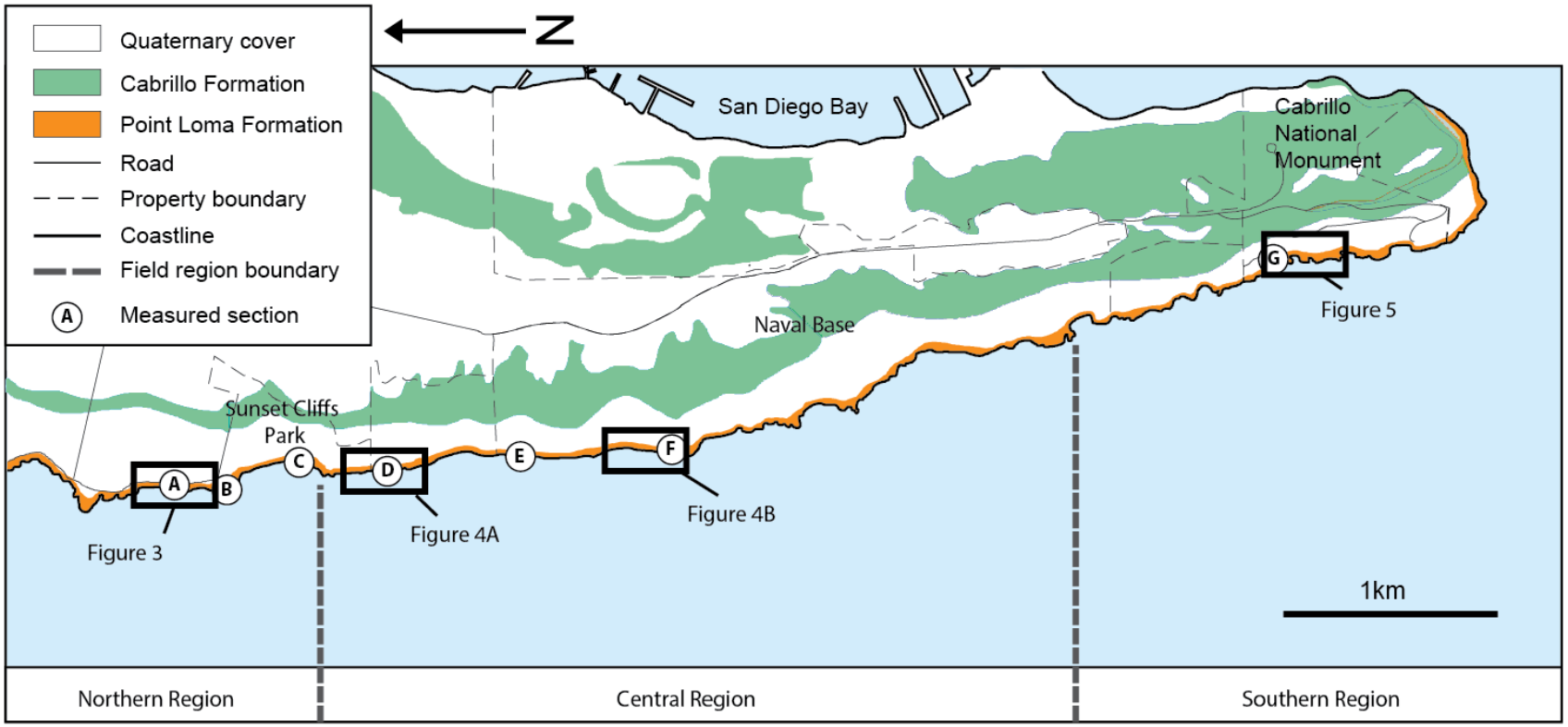

Figure 2. Geologic map of the study area. Three sub-regions are defined by large offset faults. The Point Loma Formation outcrops continuously along the west side and southern tip of the peninsula. (Modified from Kennedy and Tan, 2005 and Fleming, 2010).

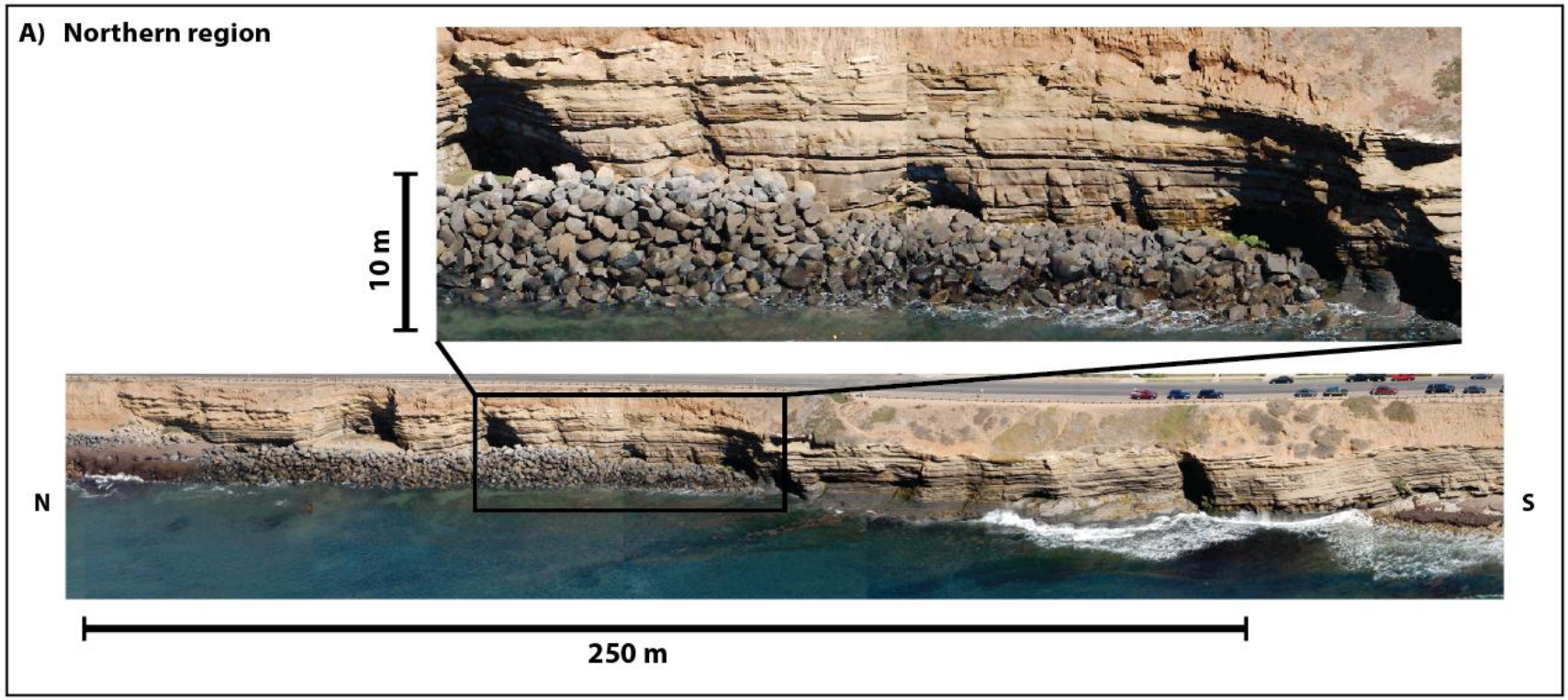

Figure 3. Photopanel of interpreted proximal lobe strata in the northern field region. (photos from the California Coastal Records Project, www.californiacoastline.org)

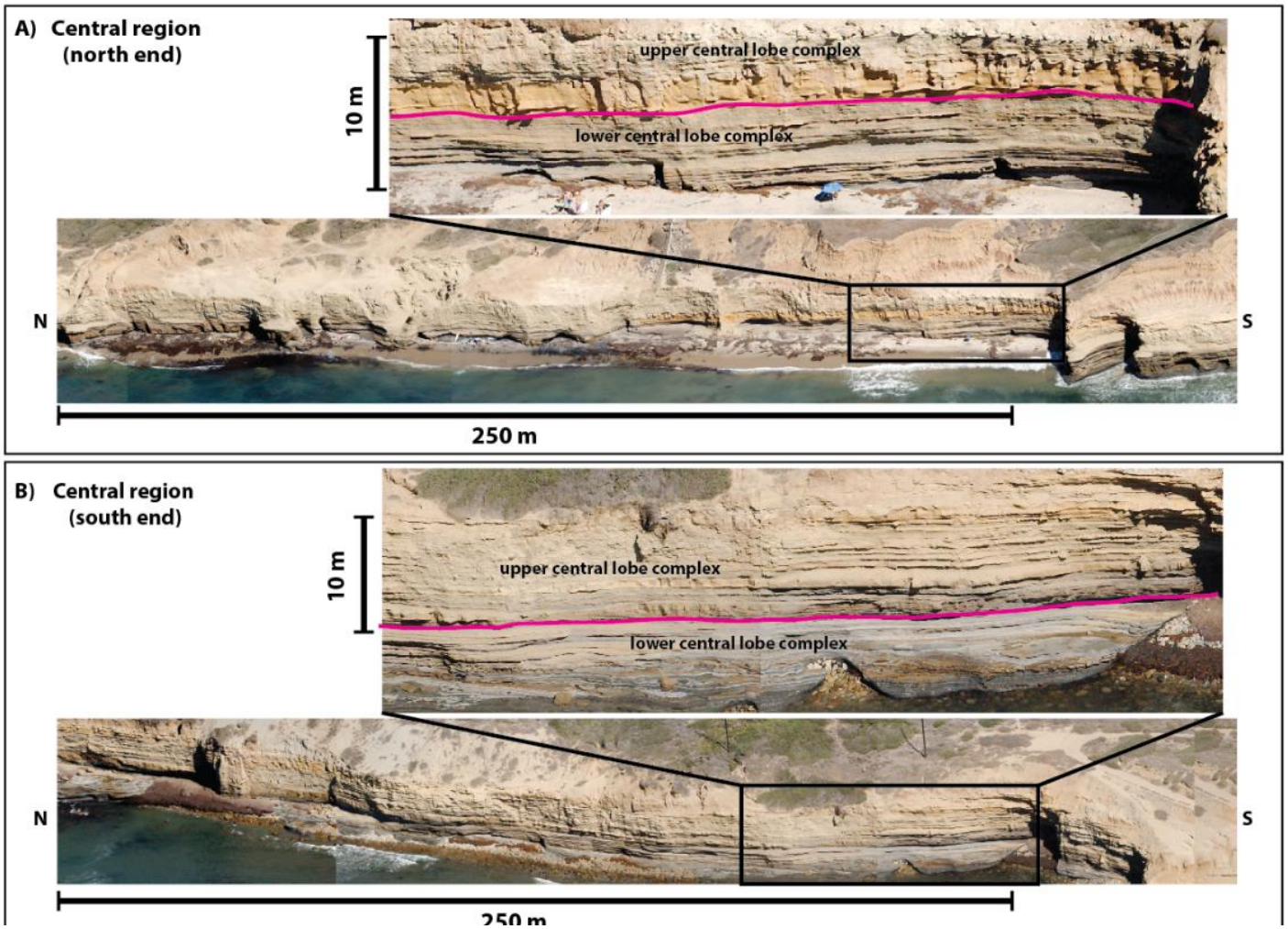

Figure 4. A) Photopanel of lobe strata in the central field region. (B) Photopanel of lobe strata in the central region; 2 km south of A (photos from the California Coastal Records Project, www.californiacoastline.org)

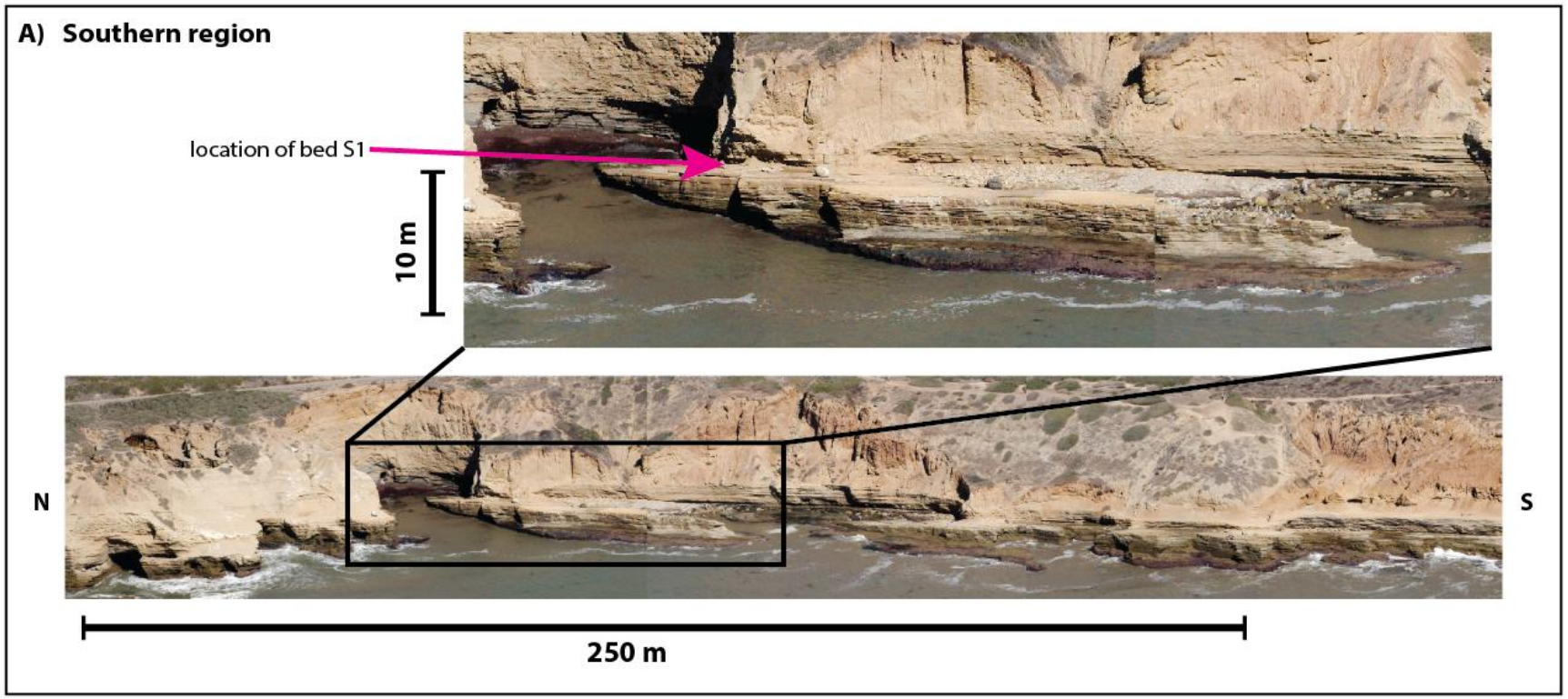

Figure 5. Photopanel of interpreted distal lobe strata in the southern field region. (photos from the California Coastal Records Project, www.californiacoastline.org)

4: Data and methodology

Deposits exposed within the study area are weakly cemented and largely undeformed. Erosion from regular wave action maintains clean surface exposure for both sandy and mud-rich strata. This allowed for detailed description of deposit characteristics including grain size, thickness, bedding surfaces, sedimentary structures, biogenic features, and soft-sediment deformation features. Individual beds were followed laterally from axis to margin over distances up to 1 km to document cross-flow variability. A bed axis is defined as the position of maximum thickness, coarsest grain size, and highest sand content in an exposed bed. The resulting dataset includes 17 stratigraphic sections with a combined thickness of 63 m. Locations of measured sections are indicated on Figure 2. Sections include full descriptions including grain size and thickness values for 575 beds and 1106 bed sub-divisions. Field measurement of grain size was carried out with a hand lens and grain-size comparator, which provides sufficient resolution to group deposits into distinct grain size classes (e.g. 125-177 microns for lower fine sand). Laboratory grain size analyses were carried out for collected samples using a Malvern Mastersizer 3000, which uses laser diffraction to measure the grain size distribution of bulk sediment samples. Initial samples comprised approximately 1 cm^3 of bulk sediment, which was disaggregated with an ultrasonic probe run at 100 kHz for five minutes to ensure complete separation into constituent grains. Sediment from prepared samples was added gradually to a wet dispersion unit to reach a target laser obscuration of 10-20%.

Each sample was measured six times per run and the particle size distribution was calculated from the average of these measurements.

5: Results

5.1. Facies

A sedimentary facies scheme is used to describe the characteristics of TFDs and associated deposits. Mud content refers to the volume percentage of particles within a deposit that are silt size or finer (i.e. <63 microns). Many of the facies in the Point Loma Formation are similar to those found in other turbidite systems where they have previously been described in detail. For completeness, Table 1 summarizes documented facies within the study area. Detailed descriptions of key facies associated with TFDs are provided below.

Structureless sandstone

Structureless deposits range from coarse to very fine sandstone that lacks primary sedimentary structures (Fig. 6A). This facies was described and measured in 126 beds. Individual structureless sandstone deposits are up to 118 cm thick. The thicknesses are well described by a lognormal distribution with the mean of the log-transformed thickness data (μ = 1.961, σ = 0.998) corresponding to a thickness of 9.4 cm. Mud content was measured for 19 samples and ranges from 17% to 39%, with a mean of 28% (Fig. 9). Grading is common but can be subtle for deposits consisting of fine to very fine sand. Lower bounding surfaces are sharp and typically flat. Basal scouring was most commonly observed for relatively thick sandstones (>20 cm) and in sections with frequent bed amalgamation. Where overlain by banded intervals (described below), this

facies commonly shows an upward-increasing abundance of carbonaceous material and/or a discrete 1-3 cm horizon containing rounded, mm- to cm- scale mud clasts and carbonaceous material (Fig. 8A). While the occurrence of mud clasts within structureless sandstone intervals is noted, intervals containing mud clasts are not classified herein as unique facies. Structureless sandstone intervals often show cross-flow variability in mud clast occurrence, and thus a facies scheme distinguishing deposits based on the presence of mud clasts would be unnecessarily complex. Laterally discontinuous clusters of cm- to cobble sized rip-up clasts occur at the base of some structureless sandstone intervals and are typically associated with local scours. Mud clast-bearing horizons near the tops of structureless divisions are most common near bed axes and typically disappear toward the bed margin within 10-75 m. Clast-on-clast contacts are uncommon in these upper horizons. Clast imbrication was apparent in very few examples near the base of the deposit.

Banded sandstone

Banded sandstone comprises fine to very fine argillaceous sandstone with distinctive, repeated alternation of cm- to mm- scale light-dark couplets (Fig. 6B). The contrast between dark and light bands results from high concentrations of platy organic material in dark bands. Organic material within dark bands is poorly sorted and shows no preferred orientation of long axes (Fig. 7A). The thickness of individual bands distinguishes banding from parallel lamination, as bands are tens of grain diameters thick or more. 316 banded intervals were measured with a maximum thicknesses of 17 cm.

Thicknesses follow a lognormal distribution (μ = 0.856, σ = 0.763) in which μ corresponds to a thickness of 2.7 cm. Banded intervals are mud-rich relative to other sandy facies, with measured mud content from nine samples ranging from 29% to 67%, with a mean of 54% (mud content is summed over light and dark bands; Fig. 9). Isolated mm- scale mud clasts were rarely observed in banded intervals.

Mudstone

Mudstone intervals can be exceptionally well-exposed in the study area (Fig 7B). 556 mudstone intervals were measured with a maximum thickness of 17 cm. The thickness data show a lognormal distribution (μ = 1.277, σ = 0.658) where μ corresponds to 4.3 cm. Well-exposed examples of this facies can be divided into upper and lower portions with different sedimentary characteristics. However, lower and upper portions were lumped together for thickness measurements, as most mudstones were not exposed well enough to distinguish between the two in the field. The lower portion of this facies consists of sandy to silty mudstone which is sometimes laminated but in most cases the original depositional fabric has been completely overwritten by bioturbation. Upper portions of mudstone intervals consist of structureless mud and typically show no evidence of bioturbation. Sparse very fine to silt-sized carbonaceous material occurs in the lower portion but was not observed in the upper structureless mud.

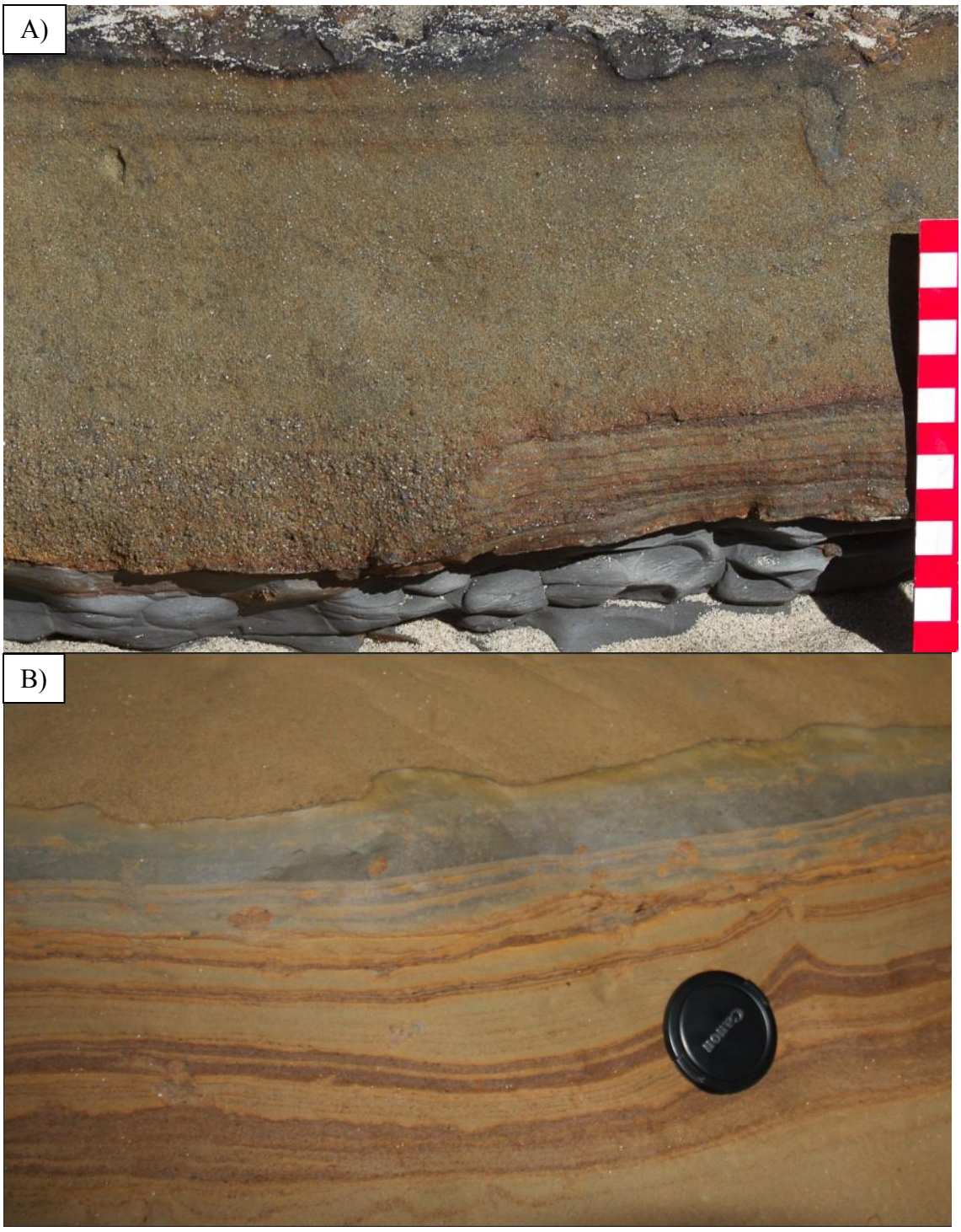

Figure 6. (A) Structureless sandstone facies located in the lower central field region. (B) Mud-rich banded sandstone with mild deformation; capped by mudstone. Located in the southern field region (section G, Fig. 2).

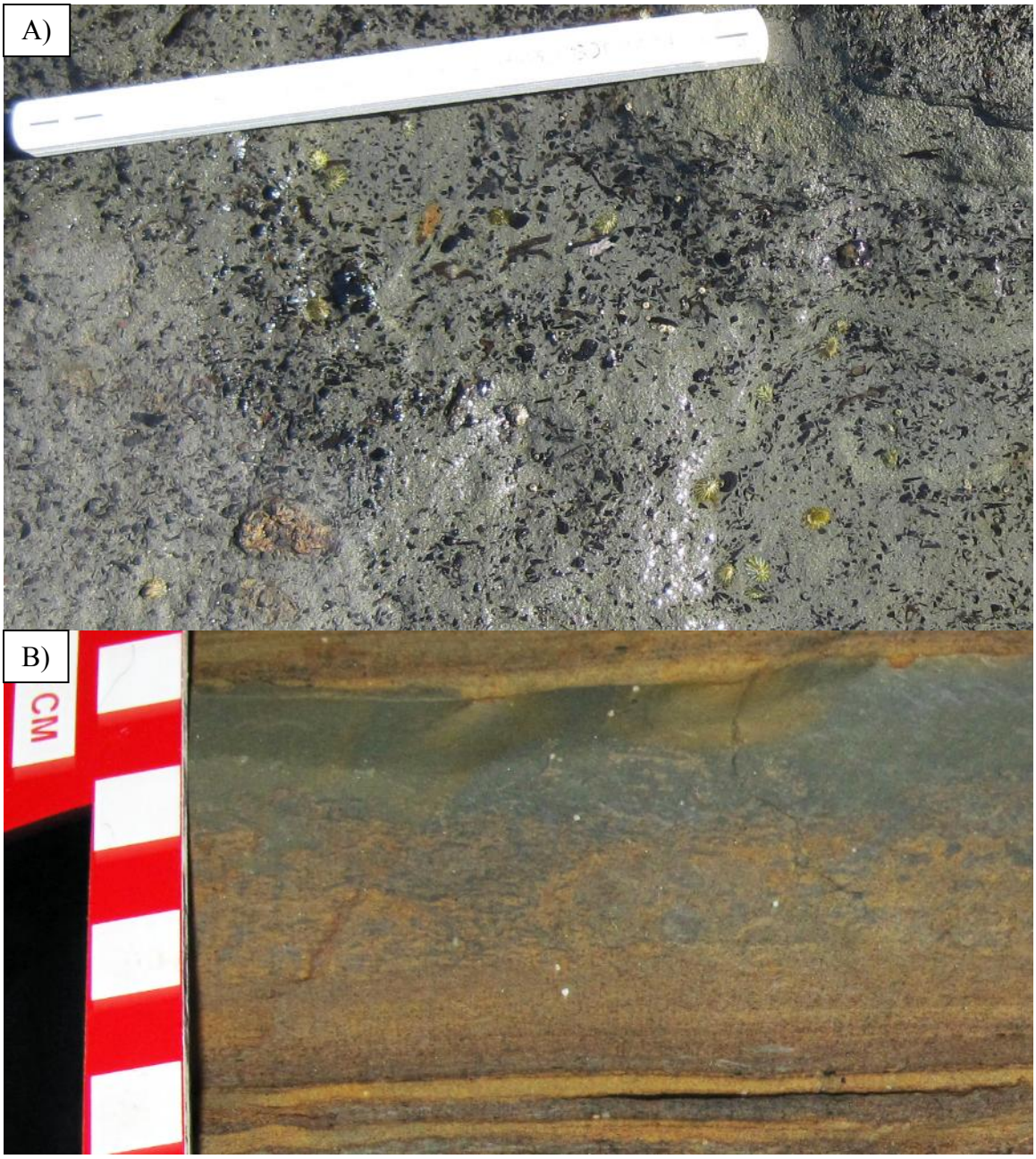

Figure 7. (A) Plan-view photo showing disorganized clasts of carbonaceous material within a ‘dark’ band. Lower central lobe complex. (B) Example of a capping mudstone division in the southern field region (Fig. 2, section G). The lower portion comprises bioturbated sandy siltstone and transitions upward to homogenous mud.

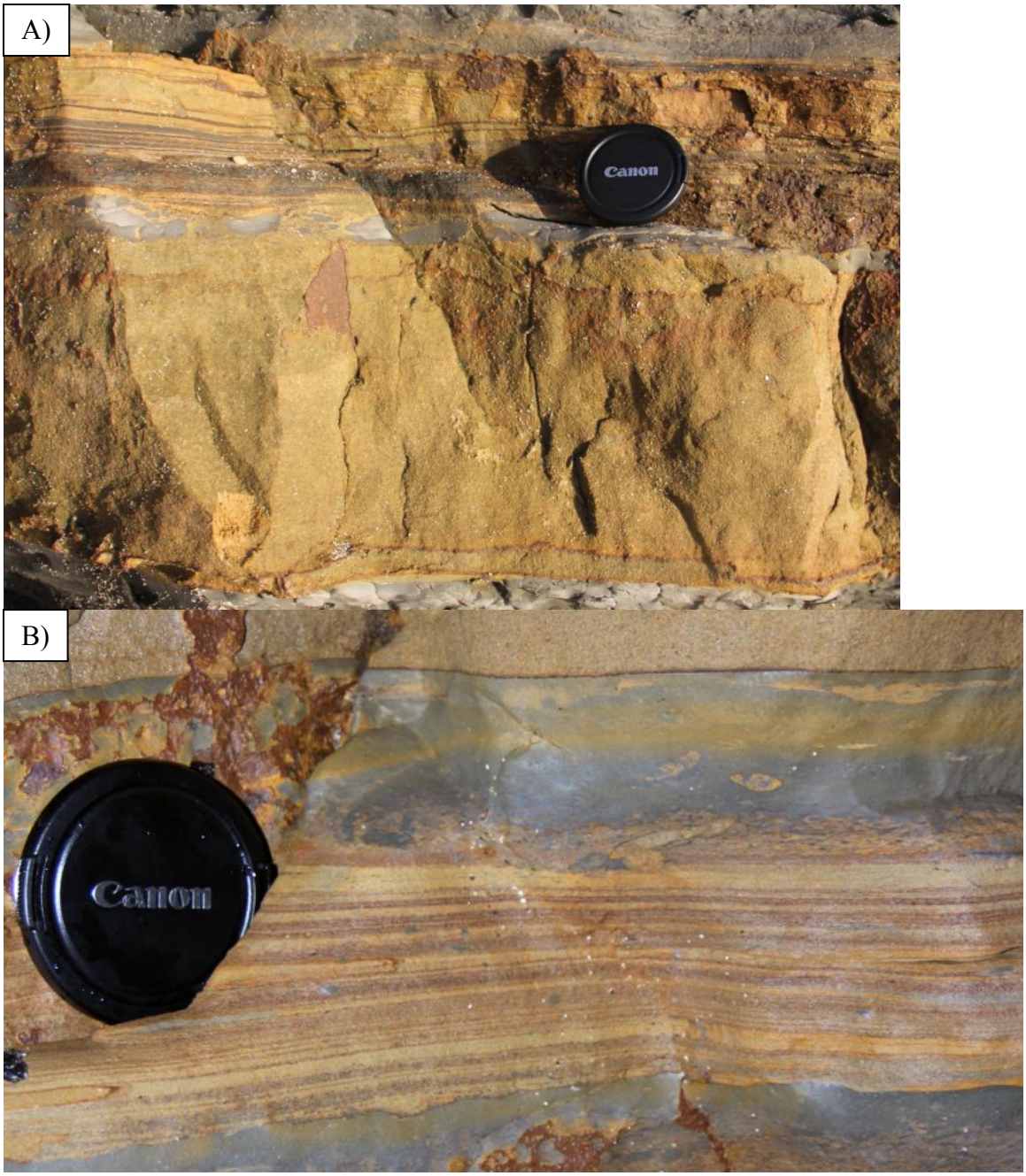

Figure 8. (A) Example of a three-component TFD (type 1), with basal structureless sandstone division, middle banded interval, and mudstone cap (Located at section E, Fig. 2). A horizon with cm-scale mud clasts and dispersed organic material marks the boundary between the structureless and banded intervals. (B) Two-component TFD (type 2) including the banded interval and mudstone cap (Section G, Fig. 2).

Name	Description	Grain size	Interpretation	Equivalent facies
Structureless sand	Sandstone deposit lacking primary sedimentary structures. Mud clasts (1-20 cm diameter) occur locally along upper and/or lower boundary, or in distinct horizons w/ organic debris	Coarse to very fine	(1) Suspension fallout (rapid); (2) collapse of sheared near-bed layers (Vrolijk and Southard, 1997; Sumner et al., 2008)	T_a – Bouma (1962) S_3 – Lowe (1982) F_7 – Mutti (1992)
Parallel laminated sand	Relatively clean sand with horizontal mm-scale parallel laminae. Laminae thickness is on the order of one grain diameter. Rare mud clasts (mm- to cm-scale) along distinct horizons	Medium to fine	Bedload reworking under turbulent flow	T_a – Bouma (1962) S_3 – Lowe (1982) F_9 – Mutti (1992)
Ripple cross-laminated sand	Relatively clean sand with ripple cross-laminae. Most common as starved ripples in mud-rich successions, or as a single train of ripples at tops of other sandstone intervals. Rare thicker (> 5 cm) packages of climbing ripples	Fine to very fine	Bedload reworking under turbulent flow	T_c – Bouma (1962) F_9 – Mutti (1992)
Banded sand	Muddy sand with repeated dark and light bands. Dark bands have high concentrations of carbonaceous debris with no preferred long axis orientation. Band thickness >> grain diameter	Fine to very fine		H2 – Haughton (2009) M_2 – Lowe & Guy (2000)
Mudstone	Finely laminated to structureless mud; can be weakly graded or ungraded		(1) Suspension fallout from dilute current; (2) consolidation of fluid mud layer	T_{de} – Bouma (1962) F_9 – Mutti (1992)
Debrite	Sand (clean to muddy) or mud. Contorted or indistinct fabric. Poorly sorted. Common clasts include shell fragments, carbonaceous debris, and/or mud clasts ranging from < 1 cm to > 1m in diameter. Sharp basal surface. Upper surface sharp to gradational, often with irregular topography	Coarse to silt (matrix)	Deposit of a cohesive debris flow, slide, or slump.	

Table 1. Description of common facies documented in the field area, with interpreted depositional processes and widely-used facies model equivalents.

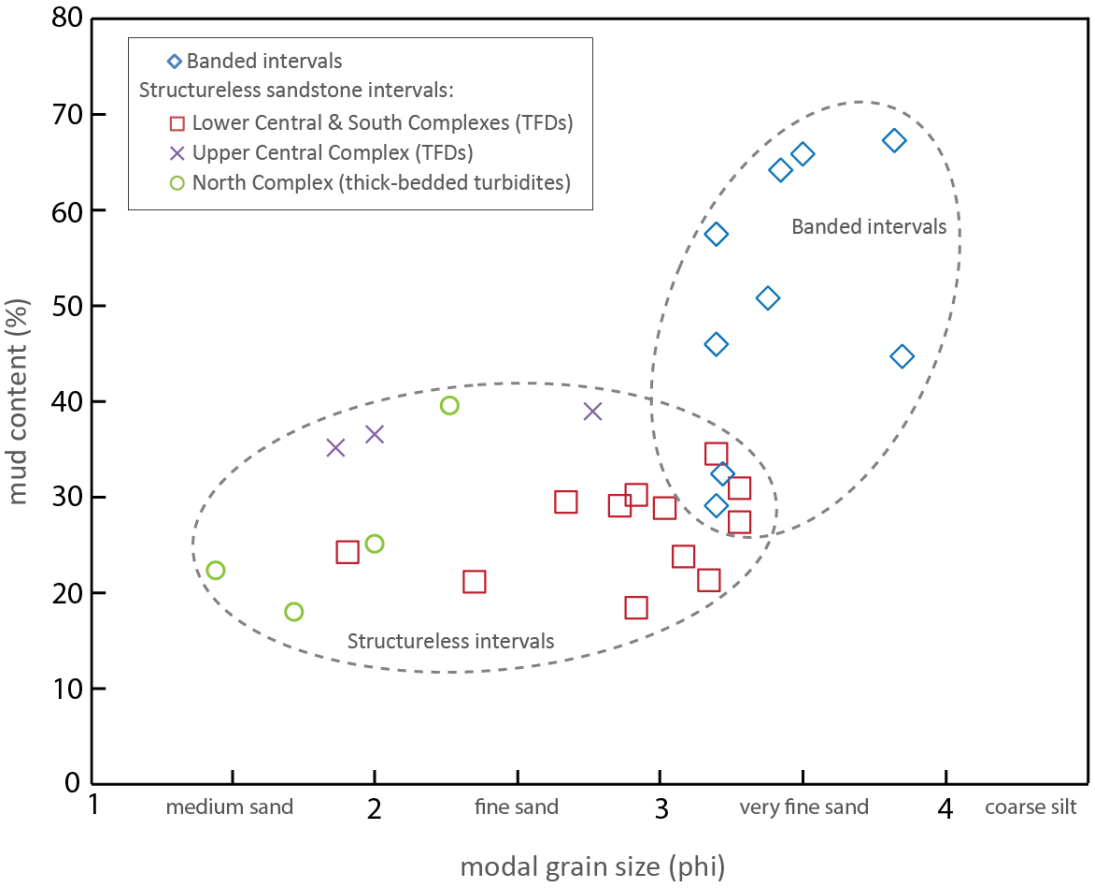

Figure 9. Mud content of structureless sandstone and banded intervals as a function of modal grain size. Grain size data are from laser particle size analysis of collected samples. Samples from structureless sandstone intervals are grouped by lobe complex and bed type.

5.2. Event beds

Transitional flow deposits identified within the Point Loma Formation are grouped into two types of event beds (Fig. 8A, Fig. 8B). The term 'event bed' is used here to refer to the deposit from a single depositional event (e.g. a turbidite deposited by an individual turbidity current, or a TFD deposited by a single transitional flow). Type 1 TFDs are composed of a basal structureless sandstone division overlain by banded sandstone and capped by mudstone. Both of the sandy divisions are thickest at bed axes and thin laterally toward bed margins. Contacts between structureless sandstone and overlying banded divisions are typically sharp, but can be gradational over 1-3 cm with an increasing abundance of carbonaceous material toward the top of the structureless sandstone division. Contacts between banded intervals and mudstone caps are gradational to sharp. Although mudstone intervals are considered as a whole for bed thickness measurements, only the lower silty portion is interpreted to be clearly linked to the same depositional event as underlying sandstone divisions. This interpretation is based on the observed presence of carbonaceous material in the lower portion, as well as observed gradational contacts with underlying banded divisions. Upper homogeneous mud portions are not clearly attributed to the same depositional event as the underlying sediment. The presence of extensive bioturbation in the lower silty mud and the absence of bioturbation in the upper portion suggest the passage of a significant amount of time prior to deposition of the uppermost homogeneous mud. Type 2 TFDs differ from type 1 deposits in that beds lack basal structureless sandstone divisions, comprising only mud-rich banded sandstone overlain by a mudstone cap.

5.3. Lateral variability within beds

The following sections utilize strike-oriented exposure to investigate cross-flow changes in geometry and composition within TFDs. Internal variability is described as a function of lateral distance from bed axes.

External and internal geometry

TFDs in the Point Loma Formation have a tapered cross-sectional geometry. Deposits are thickest at bed axes and thin toward bed margins. Internal variability is largely expressed by a major shift in shape and composition between the structureless sandstone and banded divisions (Fig. 11). Structureless sandstone divisions pinch out within 5 to 425 m from bed axes, while banded divisions are laterally continuous at outcrop scale. Rarely, thin (<10 cm) structureless sandstones were observed to thin or pinch out laterally and then reappear within relatively short distances (<10 m). Larger scale pinch-out with subsequent lateral reappearance was not observed. Measured cross-flow thinning rates (i.e. the spatial derivative of deposit thickness moving away from the deposit axis) for structureless divisions are significantly greater than those of banded divisions (Fig. 10).

Mud content

Internal changes in mud content within sampled sandstone portions of TFDs are largely associated with vertical and lateral transitions between structureless and banded divisions. Seven sample pairs were measured to compare mud contents between the bases

and tops of structureless sandstone divisions. The base-to-top increase in mud content within these intervals ranges from 3.8% to 13.5% with a mean increase of 6.9%. The vertical change in mud content between structureless and banded divisions was measured for 10 sample pairs. Mud content increases by 8.7% to 37.8% with a mean increase of 22.4%. Cross-flow changes in mud content were measured in detail for bed S1 (Fig. 11) located in the southern lobe complex. Off-axis thinning of the structureless division within this bed does not appear to coincide with an increase in mud content, which remains essentially constant over 125 meters at 27-29%. Where the structureless sandstone division pinches out, mud content at the base of the bed increases sharply to 48% with the lateral transition to the banded division.

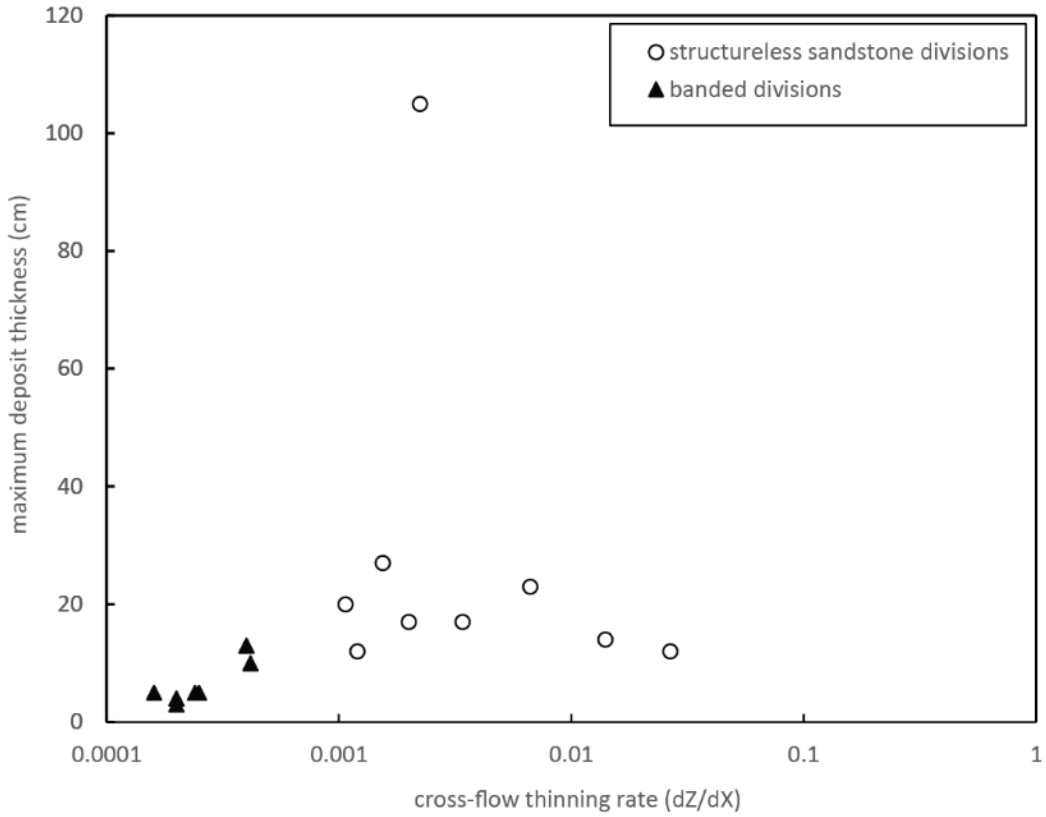

Figure 10. Plot with axis-to-margin thinning rates for structureless and banded divisions as a function of maximum deposit thickness.

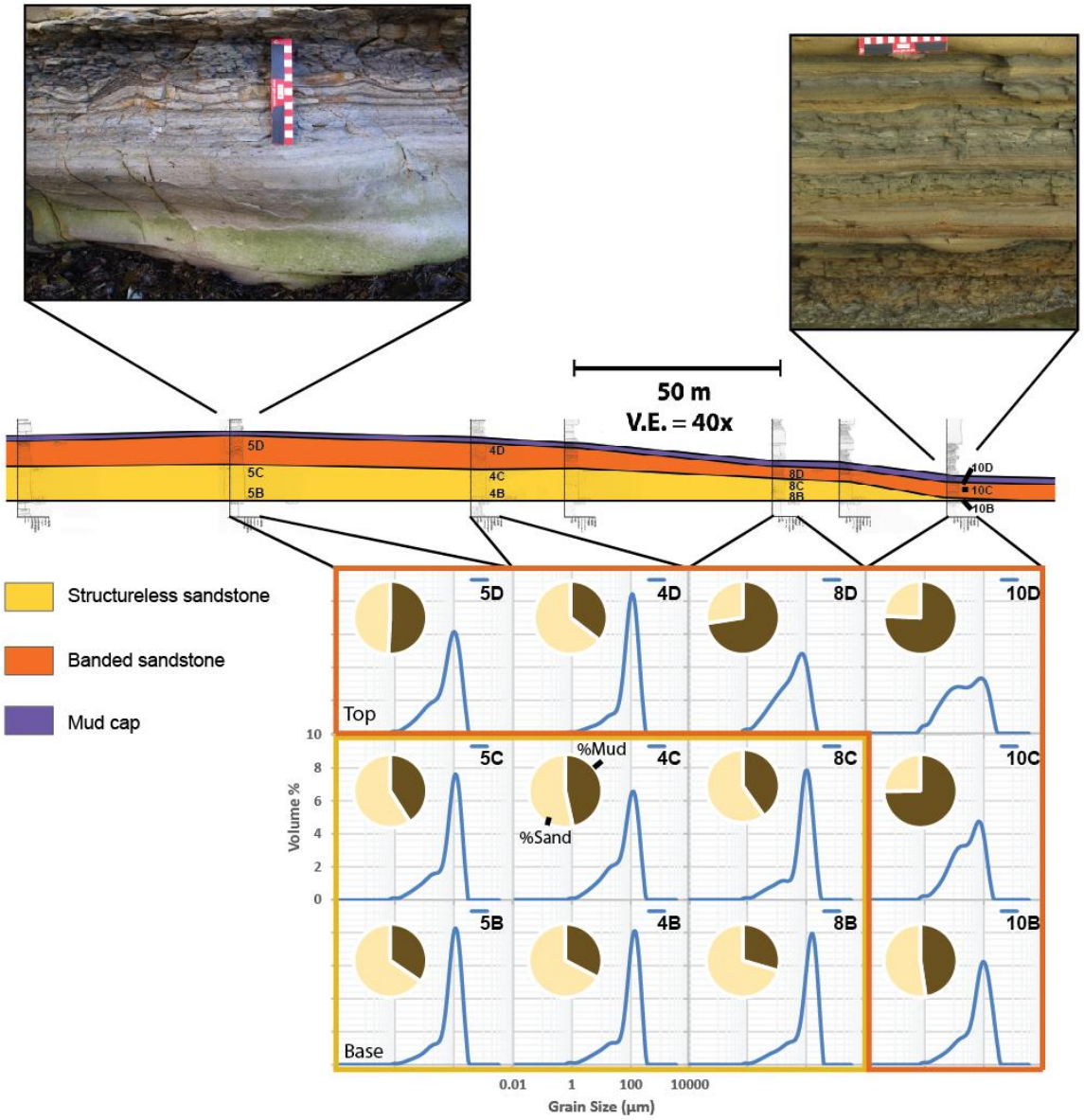

Figure 11. Cross-flow variability for a representative TFD located in the distal southern complex (bed S1, Fig. 5). Plots show vertical and lateral changes in grain size distribution, with inset pie charts for simplified observation of mud content variability. Inset photographs highlight the change in appearance from the bed axis to the location where the lower structureless sandstone division pinches out. Note the transition from deformed banding at the axis to undeformed banding toward the bed margin (transition occurs over ~100 m from bed axis).

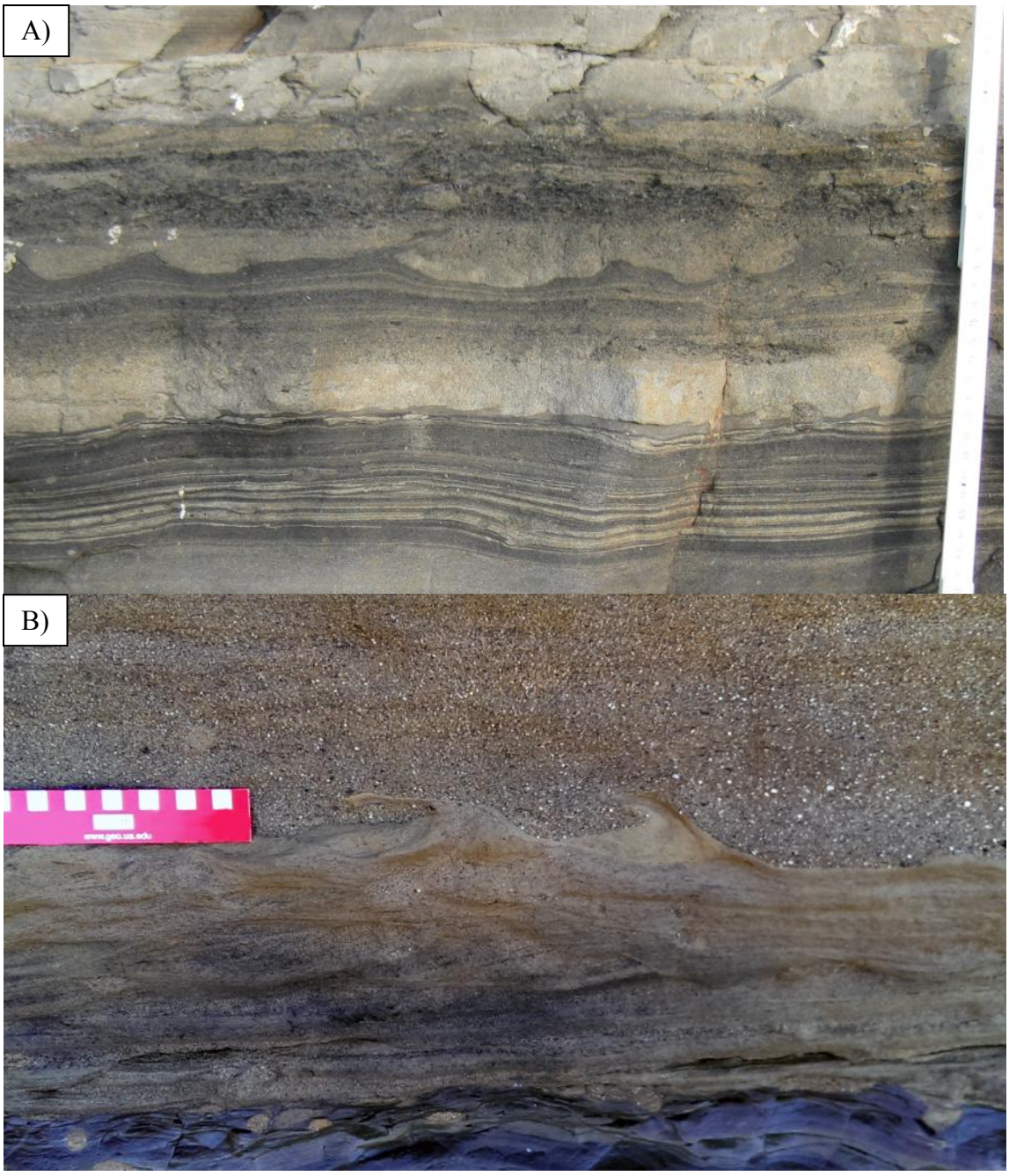

Figure 12. (A) Load structures at the interface between a banded horizon and overlying coarser sand. Measuring stick for scale (width 2 cm). Located at the base of section B. (B) Example of flame structures. North lobe complex.

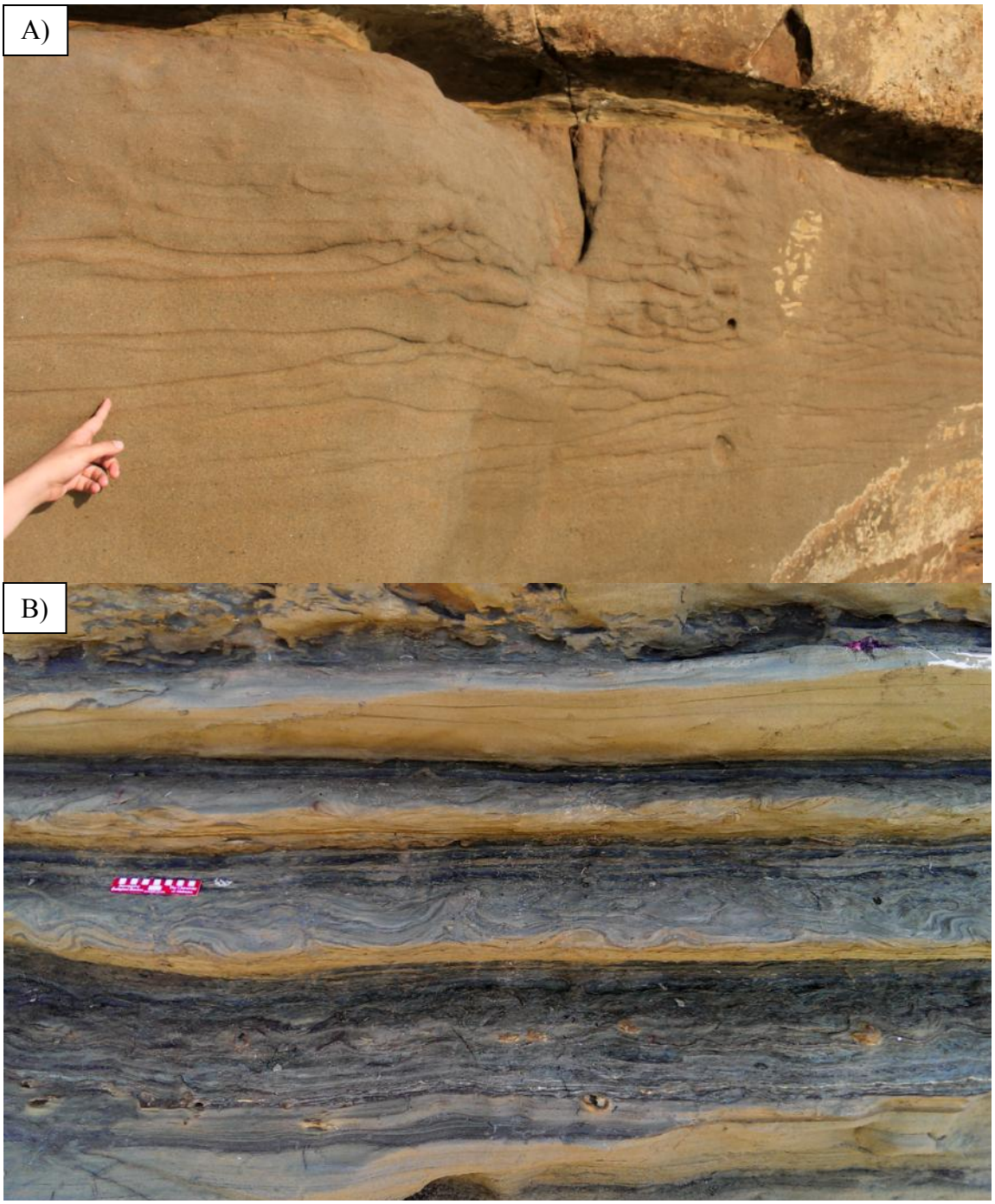

Figure 13. (A) Pervasive fluid-escape features including pipes and dish structures. North lobe complex. (B) Example of convolute lamination in thin-bedded turbidites. North lobe complex.

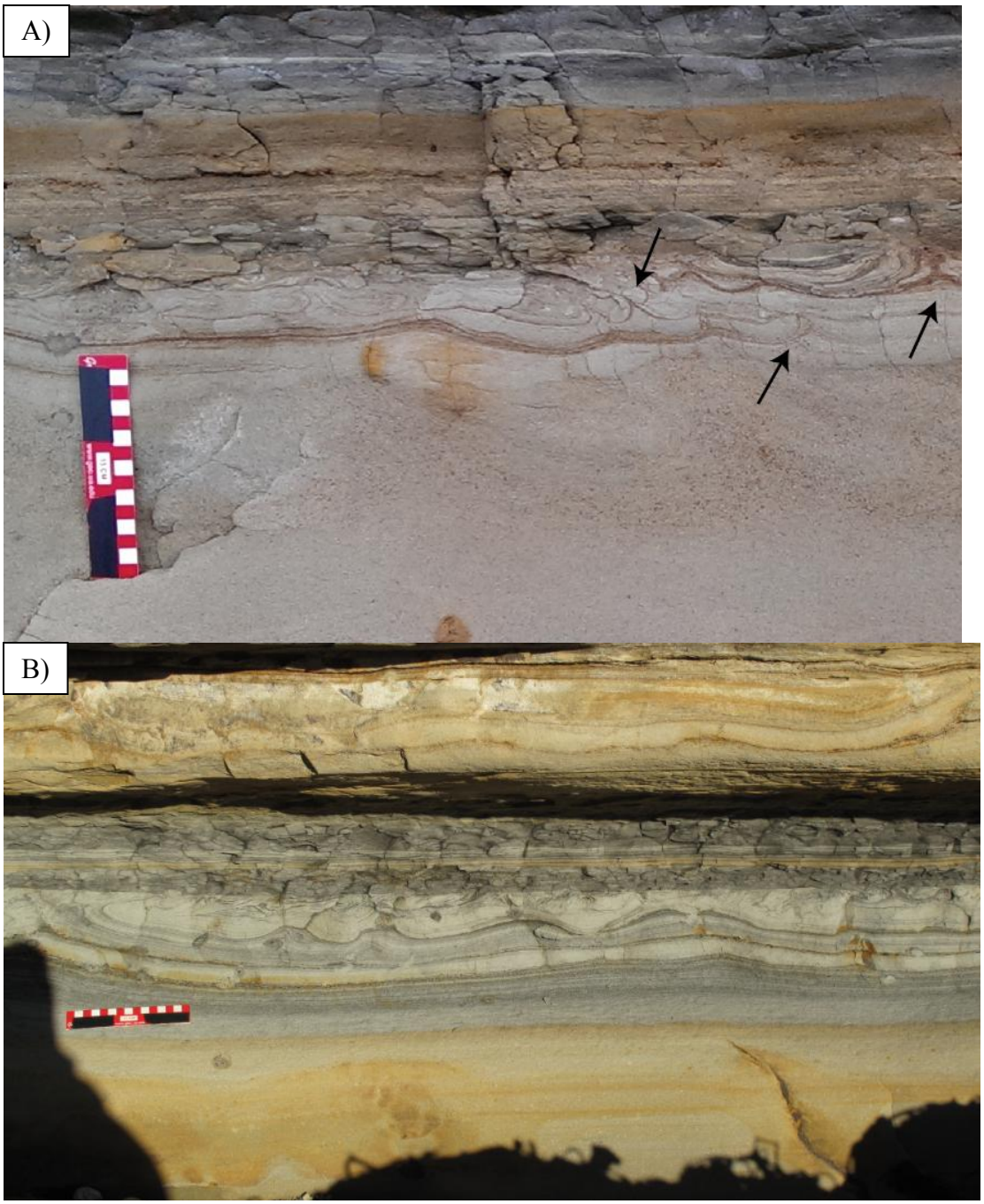

Figure 14. (A) Combined loading and fluid escape features associated with liquefaction in a banded interval. Note the lateral offset in fluid escape cusp position between subsequent bands (arrowed). (B) Deformed banding in a TFD. Note the flat surface between deformed interval and overlying mudstone. South lobe complex.

5.4. Soft-sediment deformation

Intervals displaying soft-sediment deformation features are common in lobe strata of the Point Loma Formation. Deformation is observed in both turbidites and TFDs, most often as load structures and fluid-escape structures. Load structures are expressed as undulations along the interface between a denser (at the time of deformation) layer of sediment above and a less dense layer below, and include load casts (Fig. 12A) and flame structures (Fig 12B). Fluid-escape structures are more variable in form and include vertical fluid escape pipes and dish structures in thick structureless sandstone divisions (Fig. 13A), and fluid-escape cusps in laminated and banded intervals (upward-directed, peaked folds in dark bands; arrowed in Fig. 14A). Convolute lamination is also observed in association with ripple cross-laminated divisions in turbidite successions (Fig. 13B).

The most common examples of soft-sediment deformation in TFDs are associated with banded divisions where deformation is usually expressed as gently undulating to contorted banding with associated fluid-escape cusps (Fig. 14A) and load structures (Fig. 14B). The term 'load structure' is used here to refer to both deformation features resulting from negative density gradients between static deposits (e.g. a denser sand layer overlying a lower-density mud layer) and those interpreted to result from short-lived unstable density gradients that arise during reconsolidation of liquefied deposits. Deformed banded intervals are bounded above and below by undeformed layers within the same bed. The degree of deformation in banded intervals is most intense near bed axes, particularly in beds with relatively thick (> 20 cm) underlying structureless sandstone divisions. Simple linear regression shows a positive linear relationship between

total sandstone thickness and deformed interval thickness within beds (Fig. 15). Deformation is absent to weakly-expressed where TFDs lack basal structureless sandstone divisions. Deformed intervals at bed axes are observed to gradually transition into relatively undeformed banding toward bed margins (this occurs over approximately 100 m for the example in Fig 11, inset photographs).

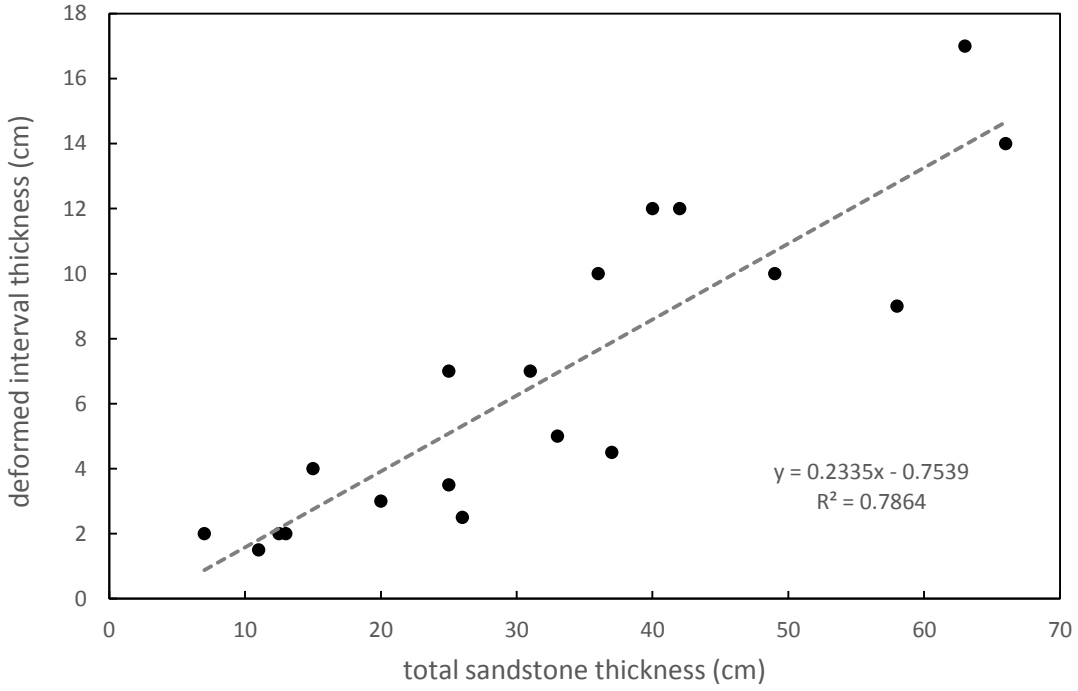

Figure 15. Plot with least square regression line for deformed interval thickness as a function of total sandstone thickness in the same bed.

5.5. Stratigraphic distribution of TFDs

Transitional flow deposits are present in all four of the studied lobe complexes. Vertical sections were measured in three complexes to assess both proximal-to-distal and axis-to-margin changes between lobe environments (Fig. 16). The percentage of measured event beds that are TFDs varies systematically between lobe environments. TFD abundance increases from 30% to 93% of the total measured thickness between the proximal turbidite-dominated northern complex and the distal southern complex. In the distal lower central complex, continuous lateral exposure was utilized to document cross-flow variability in TFD occurrence over approximately 2 km. Combined TFDs (type 1 and type 2) account for 87% of the total thickness measured at the axis of this complex. This value decreases to 80% over a distance of 500 m and then falls to 70% at the northernmost margin, largely reflecting an increase mudstone beds. The relative abundance of TFDs with lower structureless sandstone divisions (type 1) decreases significantly more from axis to margin, dropping from 58% to 26% of the total section thickness.

5.6. TFD-constructed lobe elements

Extensive high quality exposure reveals the internal organization of two lobe elements which are largely constructed by transitional flow deposits. The first occurs within the southern lobe complex (Fig. 17) and offers > 500 m of highly accessible lateral exposure. TFD stacking within the element is aggradational, with less than 50 m lateral offset between bed axes. Vertical aggradation combined with structureless sandstone

pinch-out results in a rapid decrease in structureless sandstone content away from the element axis. Structureless sandstone accounts for 42% of the measured thickness at the element axis and decreases to 14% over a distance of 125 m to the south.

The second element studied occurs within the upper-central complex and is exposed for approximately 1.4 km along depositional strike (Fig. 18). The internal architecture of this element is similar to the more distal southern element, with minor lateral offset between beds. Beds are amalgamated in the element axis where structureless sandstone accounts for 83% of the element thickness. The abundance of banded intervals and mudstone caps increases toward the element margin as beds de-amalgamate. Axis-to-margin thinning of structureless sandstone divisions reduces the coarser sandstone fraction to 36% at the southernmost exposure of the element.

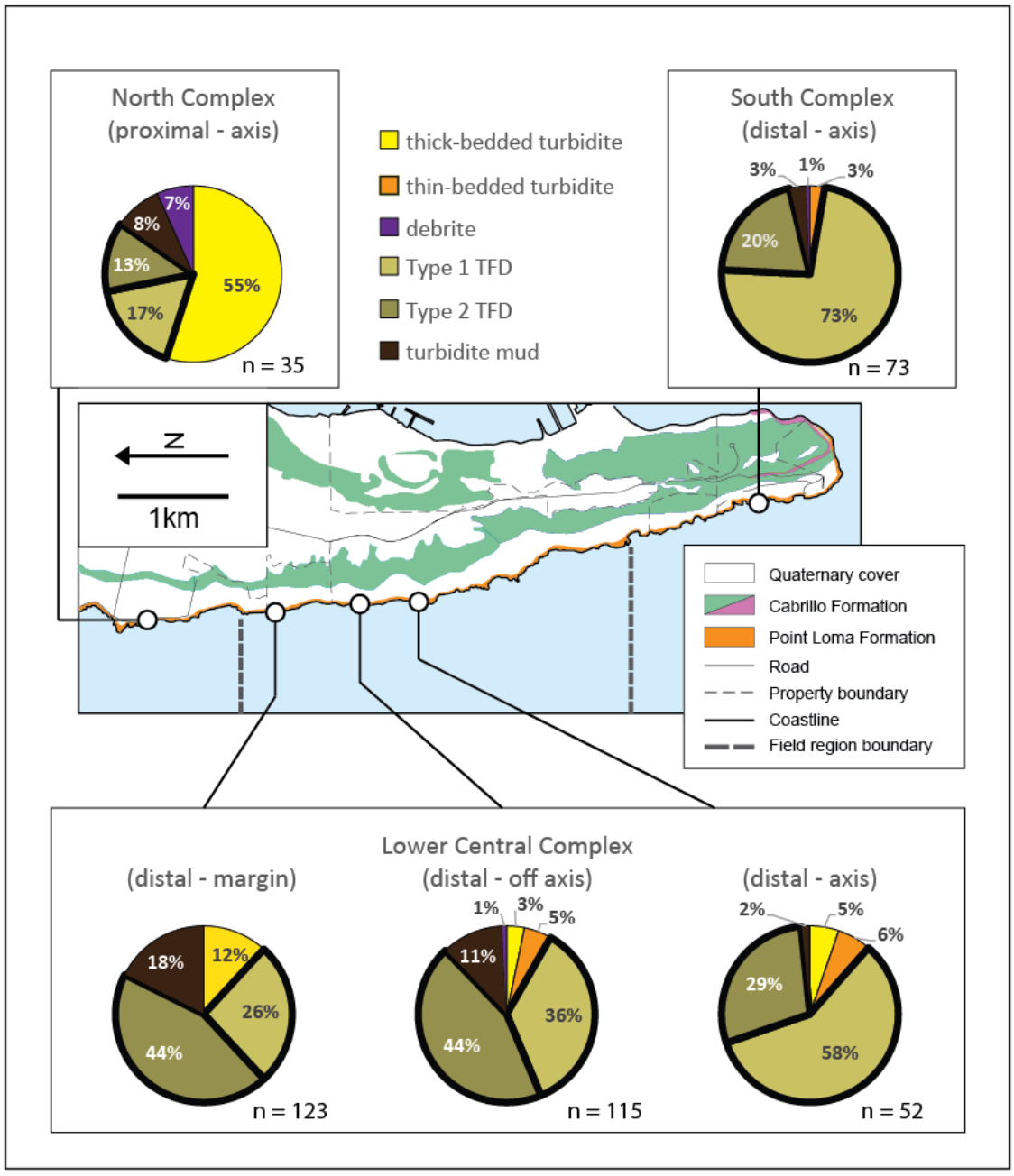

Figure 16. Relative abundance of event bed types in different lobe environments. Pie charts report the percentage of the total section thickness made up by each type of deposit.

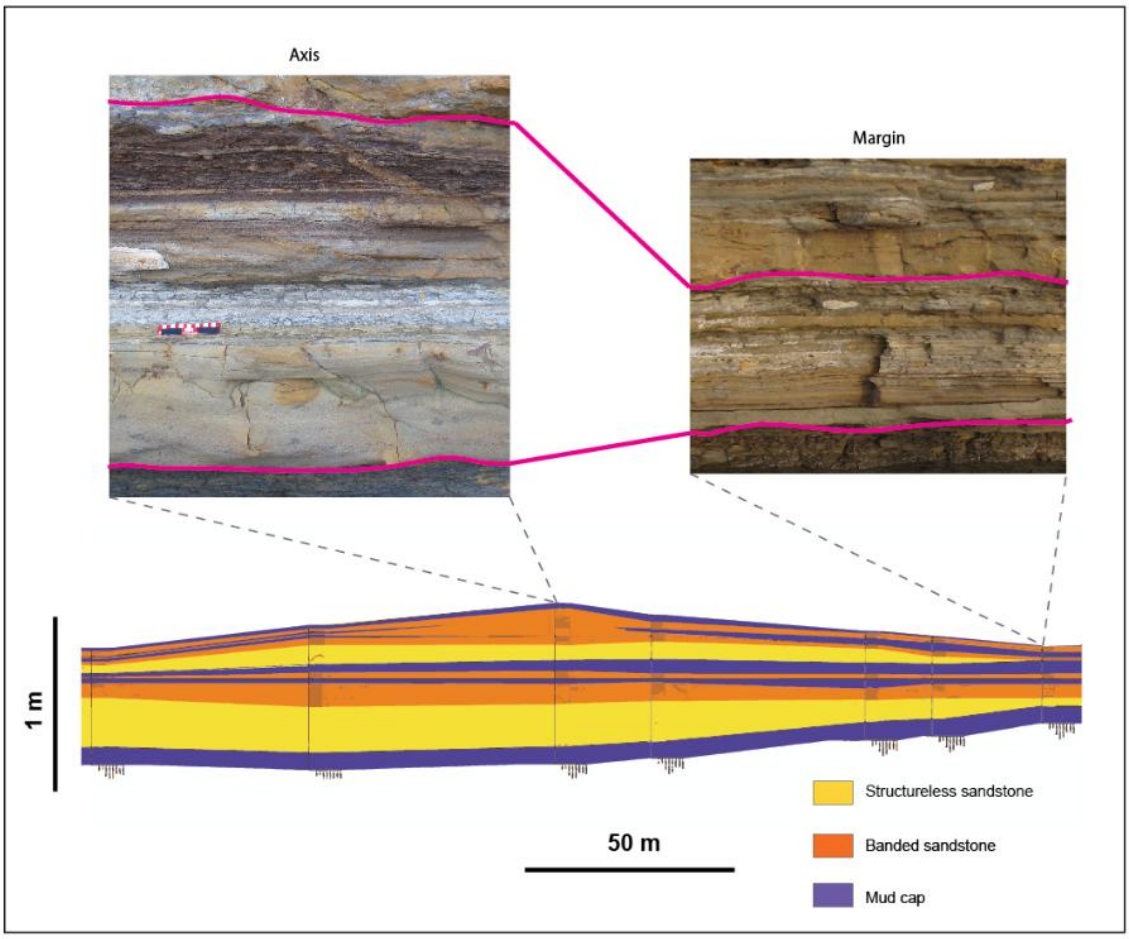

Figure 17. Correlation panel showing cross-flow variability in a representative distal lobe element. This element is located in the distal southern lobe complex (Fig. 5).

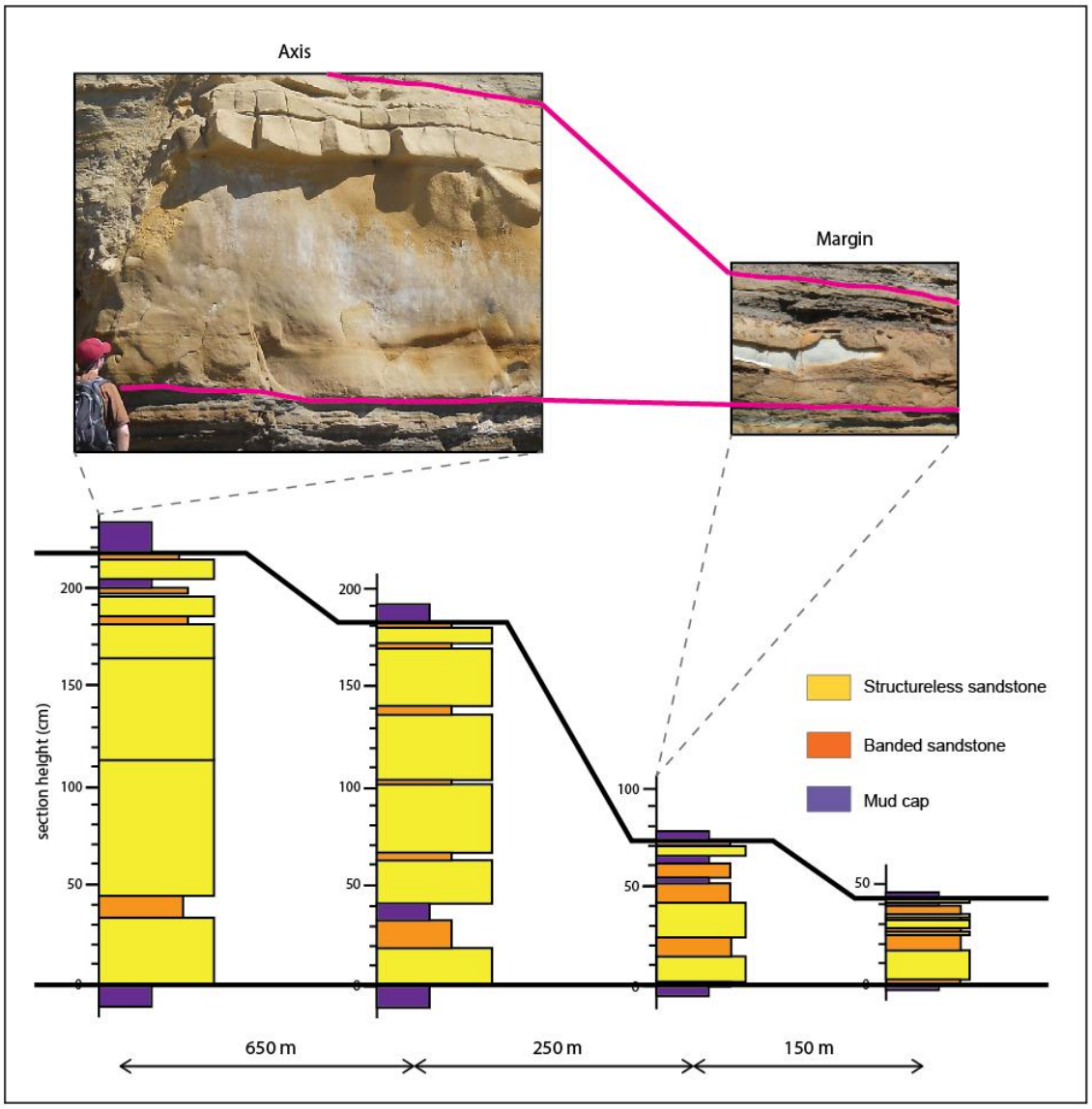

Figure 18. Correlation panel showing cross-flow variability in a representative medial lobe element. Banded divisions are largely absent in the element axis where structureless sandstone intervals are amalgamated. This element is located in the medial upper-central lobe complex (Fig. 4).

5.7. Bed thickness frequency distributions

Bed thickness frequency distributions were compared between four stratigraphic sections. High exposure quality allowed for the measurement of all beds and bed sub-divisions in each section. The frequency distribution of bed thicknesses measured in the turbidite-dominated northern lobe complex (section A) was compared with that of the TFD-dominated lobe complex in the southern region (section G). Cross-flow variability within the TFD-dominated lower central lobe complex was compared with bed thickness distributions from vertical sections at the axis (section D) and northernmost margin (section E; Fig. 19).

Cumulative frequency plots for the four measured sections are shown in Figure 20. Frequency distributions for all beds in each section are plotted. In addition, data are plotted for subpopulations of beds that have structureless sandstone divisions and those that do not. To include all beds in each section, thickness values from turbidites and TFDs were not separated. However, turbidites dominate the northern complex, comprising 55% of the section, and TFDs dominate the remaining three sections (70-78%). Median bed thickness decreases from 14 cm in the turbidite-dominated northern complex to 5 cm in the TFD-dominated southern complex. Despite the overall decrease in bed thickness between the two sections, both contain large fractions of structureless sandstone divisions, which account for 54% of the total thickness in the turbidite-dominated north complex and 40% in the TFD-dominated south complex.

An approximately lognormal distribution is indicated for each plotted distribution based on the observed linear trends. The statistical goodness-of-fit between each

measured thickness distribution and a lognormal distribution was tested quantitatively using a Lilliefors test (Lilliefors, 1967). Two out of four bed thickness distributions pass a Lilliefors test for lognormality at a high significance level ($\alpha > 0.1$; Table 2A). When these bed thicknesses are divided based on the presence or absence of structureless divisions, 5 out of 8 distributions pass the test at a 10% significance level and 7 out of 8 pass at 1% (Tables 2B and 2C).

Following Sylvester (2007), a MATLAB implementation (Tsui, 2006) of the expectation-maximization algorithm (Dempster et al., 1977) was applied to quantitatively separate thickness data from each section into two mixture components. Assuming that each distribution is a mixture of two lognormal sub-populations, this iterative method was used on the log-transformed thickness data to estimate the parameters for a two-component Gaussian mixture (Fig. 21). For the two lobe axis sections, reasonable agreement is observed between the algorithm results and distributions of bed thickness populations separated by basal facies. This suggests that bimodal bed thickness distributions for both turbidite and TFD-dominated sections result from the mixture of lognormal bed thickness populations, which are distinguished based on the presence or absence of basal structureless sandstone divisions. Significant departures from model distributions for the off-axis section of the lower central complex and complete disagreement for the margin section indicate that neither is well described as two-component lognormal mixture. The cross-flow transition from bimodal to unimodal corresponds to a decrease in the abundance of structureless sandstone intervals: these

intervals decrease from 40% of the total section thickness in the distal axis, to 33% in the off-axis section and 15% in the margin section.

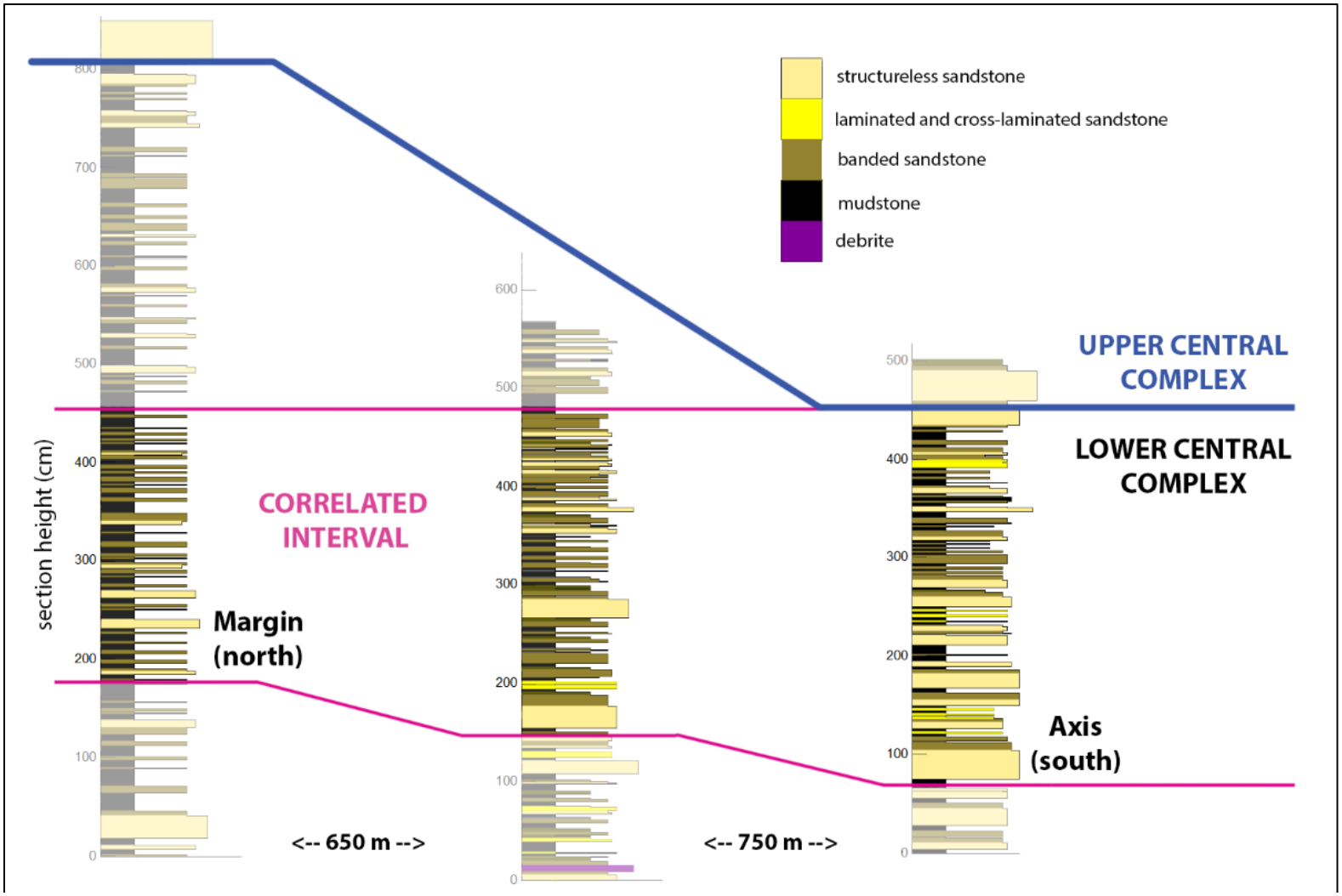

Figure 19. Measured sections and correlated interval within the lower central complex (Fig. 4).

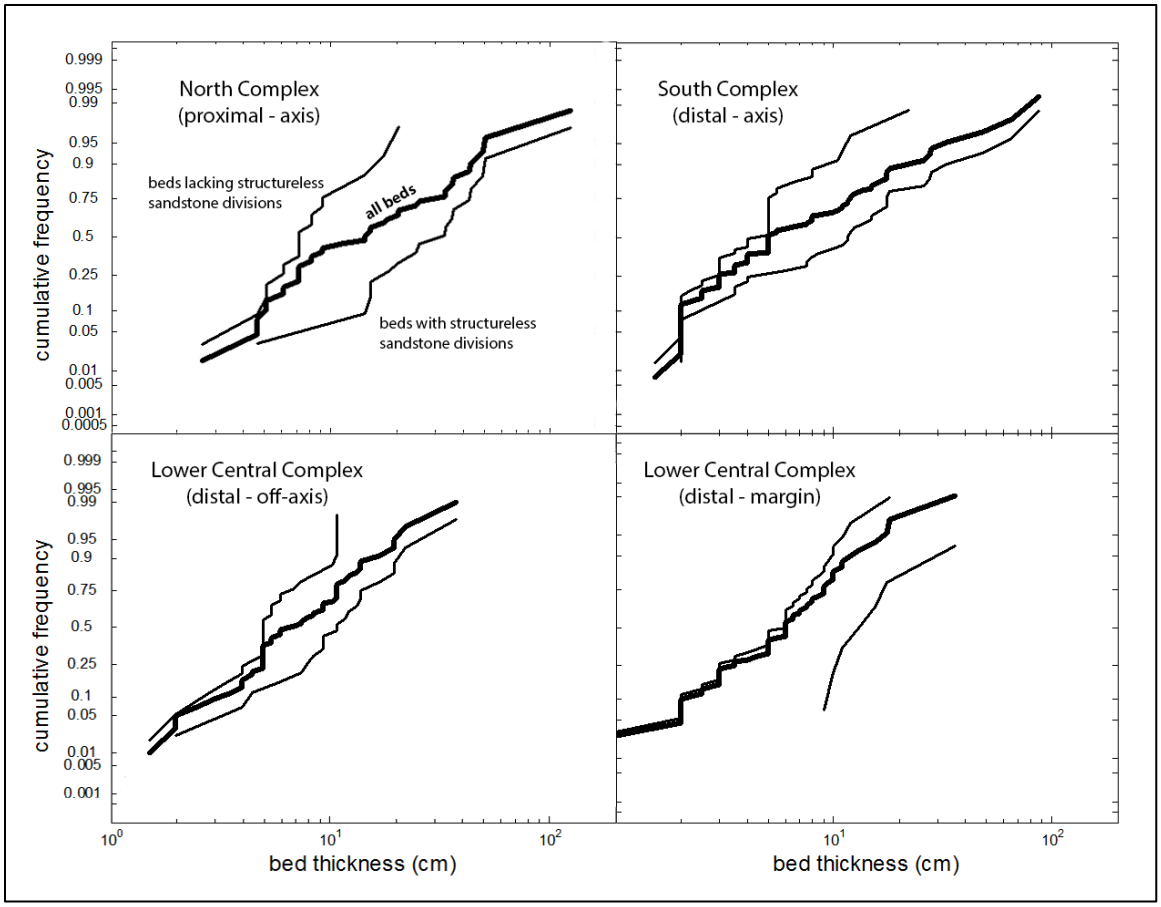

Figure 20. Cumulative frequency plots for bed thicknesses measured in four vertical sections. Each plot shows three distributions, including the distribution for all measured beds (thicker line) and distributions for beds with and without basal structureless sandstone divisions (thinner lines). Note: sections include thicknesses for both turbidites and TFDs.

Complex	Lobe Environment	Cross-flow location	Beds	Median thickness (cm)	P-value	Reject H0? (α = 0.01)	Reject H0? (α = 0.1)
North	Proximal	Axis	35	14	0.2081	No	No
South	Distal	Axis	73	5	0.0025	Yes	Yes
Central (Lower)	Distal	Off-axis	50	6.5	0.2971	No	No
Central (Lower)	Distal	Margin	54	6	0.0269	No	Yes

Table 2A. Statistics and Lilliefors test results for all beds in each section. The Lilliefors test is used to test the null hypothesis (H0) that the log-transformed thickness data are normally distributed.

Complex	Lobe Environment	Cross-flow location	Beds	Median thickness (cm)	P-value	Reject H0? (α = 0.01)	Reject H0? (α = 0.1)
North	Proximal	Axis	16	28.75	0.6261	No	No
South	Distal	Axis	35	11.5	0.5874	No	No
Central (Lower)	Distal	Off-axis	21	11	0.5143	No	No
Central (Lower)	Distal	Margin	7	13	0.5983	No	No

Table 2B. Statistics and Lilliefors test results for beds with structureless sandstone divisions

Complex	Lobe Environment	Cross-flow location	Beds	Median thickness (cm)	P-value	Reject H0? (α = 0.01)	Reject H0? (α = 0.1)
North	Proximal	Axis	19	7	0.0732	No	Yes
South	Distal	Axis	38	4.5	0.038	No	Yes
Central (Lower)	Distal	Off-axis	29	5	0.13	No	No
Central (Lower)	Distal	Margin	47	6	0.0043	Yes	Yes

Table 2C. Statistics and Lilliefors test results for beds without structureless sandstone divisions

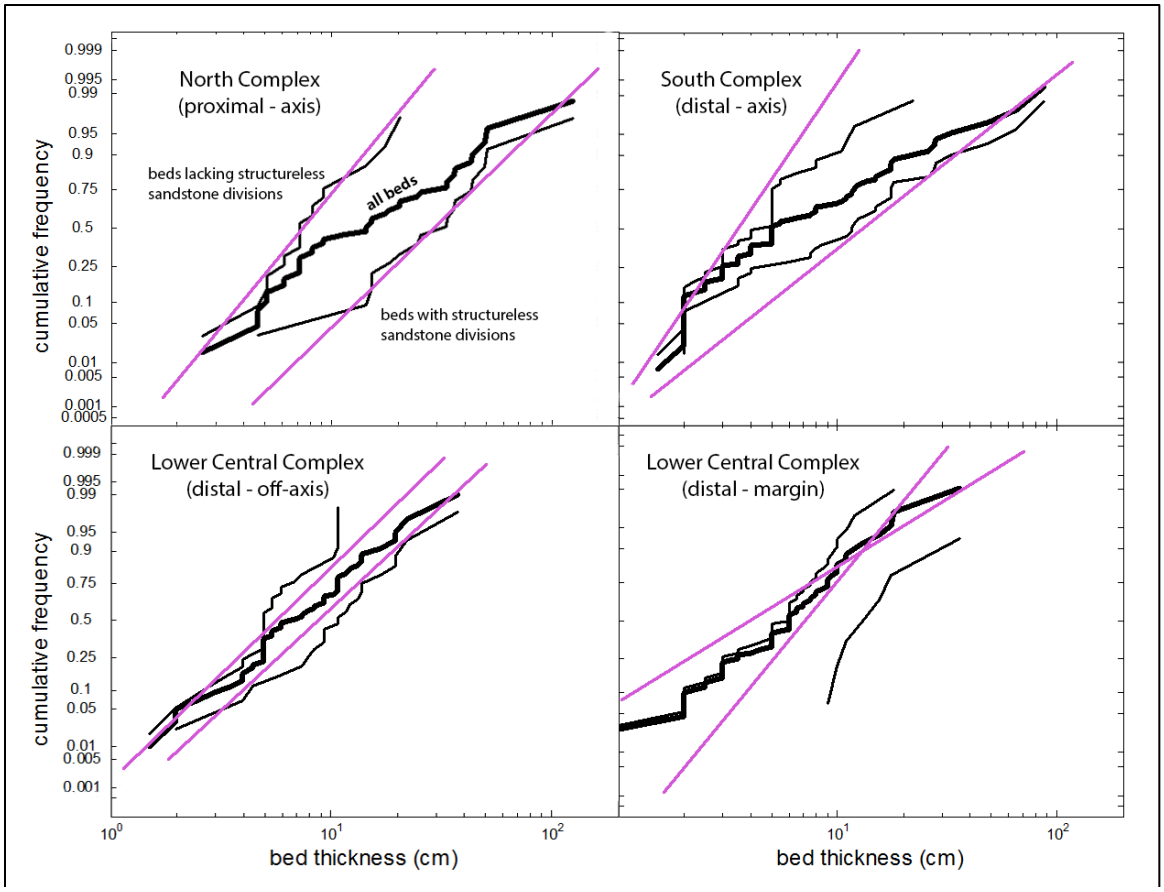

Figure 21. Cumulative frequency plots for bed thicknesses measured in four vertical sections and expectation-maximization Gaussian mixture (EM-GM) model results. Each plot shows three distributions from the measured data (black curves), including the distribution for all measured beds (thicker line) and distributions for beds with and without basal structureless sandstone divisions (thinner lines). Lognormal distributions from EM-GM model results are plotted in magenta. Note: sections include thicknesses for both turbidites and TFDs.

6: Discussion

6.1. Depositional processes

TFDs in the Point Loma Formation consistently show a bipartite internal structure in which sandstone divisions undergo a shift in composition, fabric, and shape. In the following sections, these divisions are discussed and given a depositional process interpretation based on the range of information presented by their cross-flow exposure.

Structureless sandstone

These deposits are analogous to structureless sandstone divisions of widely-used turbidite models (e.g. T_a, Bouma (1962); S3, Lowe (1982)) and models for hybrid event beds (e.g. H1, Haughton et al., 2009). Laboratory experiments have shown that structureless deposits can be produced from relatively high-concentration turbidity currents, where aggradation rates are sufficiently rapid to suppress the development lamination via bedload reworking (Kuenen, 1966; Arnott & Hand, 1989; Vrolijk & Southard, 1997; Leclair & Arnott, 2005; Sumner et al., 2008). Occurrences of mud clasts along discrete horizons and occasional faint horizontal laminae within these intervals suggest incremental, layer-by-layer deposition. Documented flute casts, scours, and local concentrations of rip-up clasts near bed bases suggests that some flows were at least initially energetic and turbulent.

Despite having lower mud contents compared to banded sandstones, the amount of mud present in structureless sandstone divisions is significantly larger than what would

be expected via selective settling of grains from a depositing turbidity current. Cumulative distribution curves for structureless sandstones show a consistent fine tail in which the bottom ~20-25% of the grain size distribution varies little between samples (Fig. 22). Lyons (2004) documented a ubiquitous fine tail comprising approximately 25% of the sediment volume for structureless sandstones in the Miocene Capistrano Formation. This percentage was shown to be consistent with the theoretical maximum amount of fine sediment that might trapped in pore spaces of rapidly deposited coarser sand. It is proposed here that such a threshold of mud content might be used as a criterion to identify candidates for structureless sandstones that were deposited by transitional flows. Setting this threshold at a maximum of 25% indicates that the mud content in 8 of 19 sampled structureless sandstones in the Point Loma Formation might be explained by trapping alone. 11 of 19 samples have mud contents between 27% and 39%, suggesting that additional mechanisms contributed to the increased amount of mud deposited with sand. Reduced mixing and inefficient grain segregation related to transitional flow behavior are considered here to be strong candidates for explaining this increased mud content; this is further supported by the observation that 10 of 11 samples with mud contents over 25% are overlain by mud-rich banded intervals.

Mud-rich banded sandstone

Deposits displaying repeated couplets of light and dark bands have been described in association with matrix-rich strata in a variety of submarine fan systems worldwide (Lowe and Guy, 2000; Sylvester and Lowe, 2004; Barker et al., 2008; Haughton et al.,

2009). Lowe and Guy (2000) propose that lighter bands are formed via settling of non-cohesive sand and silt particles, and that darker bands deposit as a result of turbulence suppression from the repeated build-up of cohesive fines near the base of a current.

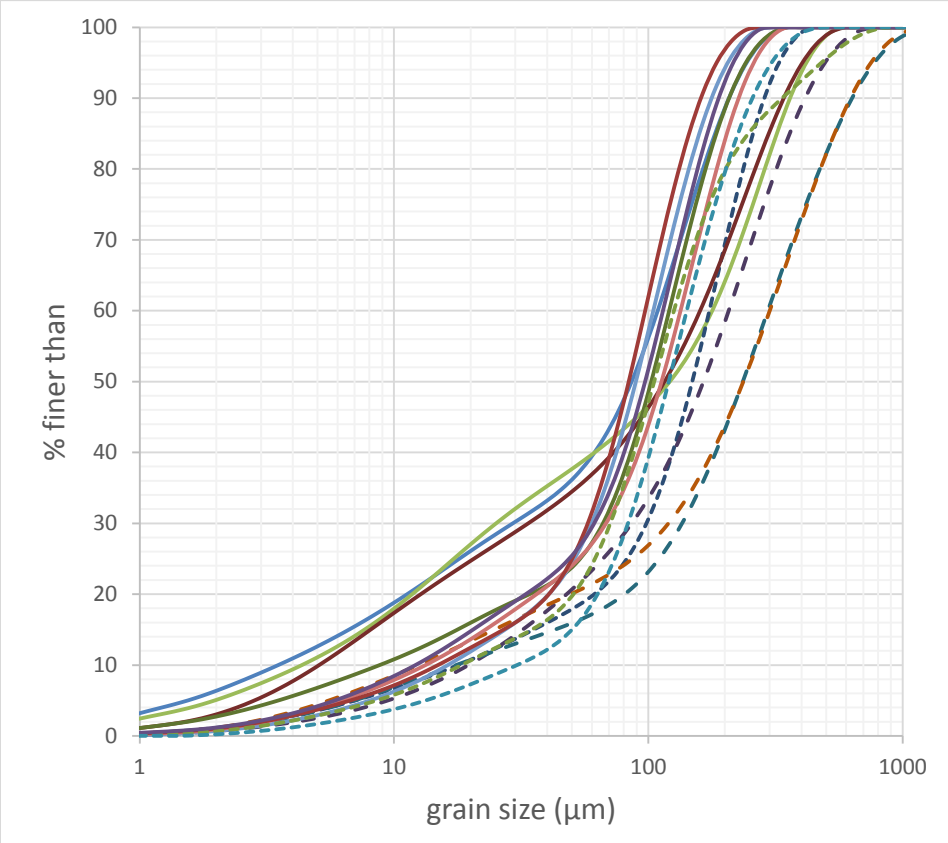

Figure 22. Cumulative grain size distributions for structureless sandstone divisions. The fine tail can be identified visually by the change in slope and low inter-sample variability for the bottom 20%-30% of each distribution curve. Samples with less than 25% mud content are indicated by dashed curves.

Proposed mechanisms for the development of banding have not been reproduced in laboratory experiments, and thus the origin of banded fabrics remains an open

question. This is the first study describing the cross-flow geometry and lateral extent of mud-rich banded intervals. The lateral continuity of these intervals suggests that the shift in depositional behavior responsible for banded deposits is associated with decreased velocity and flow expansion in unconfined distal lobe settings. In addition, the high mud content in banded divisions indicates a decrease in mixing and inefficient segregation of sand and mud during deposition.

Carbonaceous debris & mud clasts

Fragments of carbonaceous plant material and mud clasts are commonly observed in hybrid beds and TFDs, and the character and distribution of such features within beds have been used to propose both local and upstream sources for cohesion-inducing fines (Talling et al., 2004; Haughton et al., 2009; Hodgson, 2009). In the distal lobe strata described here, the scarcity of erosion surfaces and preservation of extensive mud caps beneath structureless sandstones makes it difficult to interpret flow transformation as the result of local erosion and incorporation of fines. Capping mud intervals rarely contain significant amounts of carbonaceous debris; that which is present is significantly finer in size than what is seen in banded divisions. Macroscopic carbonaceous material is similarly absent within mud clasts documented at the interface between structureless and banded divisions. Most of the mud fraction deposited with the sandstone divisions is thus interpreted to have an upstream origin.

'Core and drape' geometry

A characteristic feature of Point Loma TFDs is the contrast between internal structureless and banded divisions, where the transition between the two coincides with a shift in deposit geometry and composition. This internal shape resembles the "core and drape" geometry typical of thick-bedded turbidites (Hirayama and Nakajima, 1977; Talling, 2012b), in which a relatively thick "core" comprising intervals attributed to high-density turbidity currents (e.g. Bouma T_a, T_b) is encased by an extensive 'drape' of ripple to planar laminated turbidite sandstone and siltstone (e.g. Bouma T_c, T_d). This difference in shape is consistent with other observations that suggest differences between high-density and low-density turbidite divisions; these include the common bimodality in bed thickness frequency distributions and inflections in the relationship between bed thickness and grain size that have been documented for turbidite systems worldwide (Sadler, 1982; Talling, 2001; Sylvester, 2007). Talling (2012b) proposes that the 'core and drape' geometry may be a fundamental characteristic of turbidites. The observation of a similar internal geometry for the TFDs studied here suggests that the 'core and drape' architecture is not unique to the deposits of fully turbulent flows. It is proposed here that this geometry reflects a contrast in depositional behavior between distinct stages of deposition from waning flows.

Grain size breaks and abrupt changes in mud content

Another feature that is commonly observed in both turbidites and the TFDs studied here is an abrupt shift in grain size and/or mud content between structureless

sandstone intervals and overlying deposits. For turbidites, sand-sand grain size breaks are common between lower structureless to parallel laminated and upper ripple cross-laminated divisions (e.g. Bouma, 1962; Lowe, 1982; Mutti, 1992; Kneller and McCaffrey, 2003; Sylvester and Lowe, 2004). Occurrences of mud clasts along grain size boundaries and truncation of underlying laminae may suggest that these grain size breaks represent phases of sediment bypass (Talling, 2012b). However, mud clasts at the transition from structureless to laminated sand can also represent a transition from deposition via suspended load fallout to tractive flow deposition (i.e. where mud clasts are transported as bedload). Bypass periods have been observed in laboratory experiments following the deposition of structureless to planar laminated deposits, prior to the onset of deposition for ripple cross-laminated intervals (Sumner et al., 2008). The transition between the structureless sandstone and banded divisions documented in this study is marked by an abrupt increase in mud content, but a significant shift in modal grain size for the sand fraction across this surface was not observed. This may suggest that there was little to no hiatus between the structureless and banded intervals and that the associated transition in depositional behavior within the flows was abrupt.

6.2. Soft-sediment deformation and TFD permeability

Most examples of soft sediment deformation in hybrid beds and TFDs have been described from drill core or limited outcrop exposure (Lowe and Guy, 2000; Sylvester and Lowe, 2004; Hodgson, 2009; Kane and Ponten, 2013). The extensive lateral exposure of TFD-dominated strata in the Point Loma Formation provides an opportunity to better

understand relationships between soft sediment deformation and the initial configuration of sediment in TFDs. Analysis of soft sediment deformation features in this study is focused on identifying three conditions required for deformation: (1) a deformation mechanism; (2) a driving force that propagates deformation and (3) a trigger that reduces the strength of the deposit and initiates deformation (Owen et al., 2011).

Deformation features documented for TFDs in the Point Loma Formation indicate two dominant deformation mechanisms: (1) liquefaction, in which a loss of deposit strength and susceptibility to fluid-like deformation result from the transfer of grain support to pore fluid, and; (2) subsidiary fluidization, in which gains are supported by fluid drag from escaping pore fluid. Once a deposit becomes liquefied, the grain framework is gradually reestablished by the settling of grains through the pore fluid (Lowe, 1975; Allen, 1982). Closer packing of grains during re-sedimentation is interpreted to have displaced excess pore fluid upward, where local fluidization occurred in response to lower-permeability layers within banded horizons. Lateral shifts in the location of fluid-escape cusps between bands suggest preferential fluid flow along higher-permeability layers (Fig. 5E). The combination of liquefaction and local expansion of fluidized sediment in isolated fluid-escape zones generated unstable density gradients, resulting in downward migration of adjacent denser sediment and amplification of deformation structures (Allen, 1982; Nichols et al., 1994; Owen, 1996).

Liquefaction requires an increase in pore fluid pressure by the action of a trigger. One plausible trigger from which elevated pore pressure can arise is the combination of

high sedimentation rates and low-permeability layers (Stromberg and Bluck, 1997; Moretti et al., 2001; Flemings et al., 2008), which inhibit dissipation of excess pore fluid pressure. Another potential trigger is cyclic pressure fluctuation from earthquake shaking, which has been invoked to explain soft-sediment deformation in a variety of depositional environments (e.g. Sims, 1973; Leeder, 1987; Obermeier, 1996; Moretti, 2000; Shiki et al., 2000). Paleoseismicity is a plausible trigger in a forearc basin setting and thus might explain some of the deformation observed in the Point Loma Formation. Most of the deformation within TFDs, however, is interpreted to have been triggered by intrinsic sedimentary processes rather than earthquake shaking based on the following observations: (1) the limited cross-flow extent of deformed intervals; (2) the frequent vertical repetition of deformation in layers of similar lithology, and; (3) the association of deformed intervals with interpreted lobe environments in which alternating sandy and mud-rich layers were deposited relatively frequently. The greater intensity of deformation observed at bed axes in the studied TFDs is consistent with larger fluid volumes trapped in pore spaces at the thickest parts of beds; draping by mud-rich banded intervals and mudstone caps likely served to inhibit consolidation of basal structureless sands (Fig. 23). The increasing load from continued sedimentation is interpreted to have outpaced pore pressure dissipation, eventually leading to a reduction in strength and increased susceptibility to deformation. This deposit configuration and associated deformation is common for TFD-dominated strata in the Point Loma Formation and may be characteristic of TFDs in other locations.

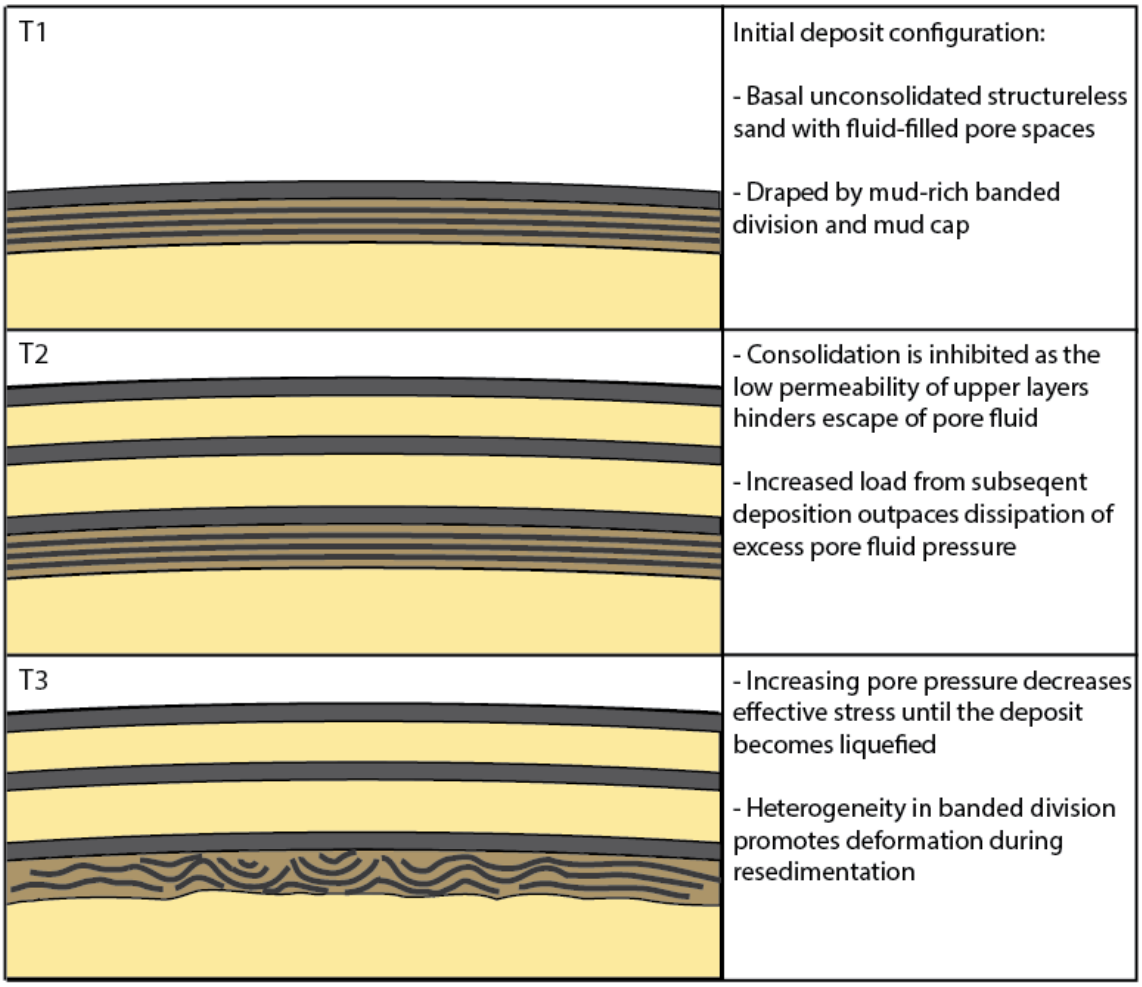

Figure 23. Simplified cartoon depicting the genetic model for soft-sediment deformation in the studied TFDs.

6.3. Depositional model for individual TFDs

An interpreted sequence of depositional processes responsible for building an idealized TFD is summarized as follows: (1) First, the structureless division is deposited layer-by-layer by the settling of the sand fraction from a high-concentration basal layer within a mud-rich, density stratified flow (Figure 23A). This high-concentration basal layer is sensitive to pre-existing topography and preferentially deposits sediment along subtle topographic lows. As the flow decelerates, finer grained sediment and platy organic material accumulate in this basal layer and are increasingly incorporated into the underlying deposit. Mud clasts within the flow are unable to settle through the dense suspension at the base of the flow due their buoyancy and relatively large size, and instead deposit at the top of the structureless sand interval. (2) The banded interval deposits during a subsequent flow stage in which reduced flow velocity and flow expansion coincide with significantly reduced mixing and poor segregation of sand and mud (Figure 23B). The repeated alternation of light and dark bands suggests the influence of some internal dynamic during this phase, but the exact nature of banding is currently unknown. (3) After deposition of the banded interval, an extensive mud cap deposits from the remaining suspended fines. Due to ubiquitous bioturbation in mudstone intervals, it is unclear whether deposition occurred by direct settling of suspended sediment or via the consolidation of a fluid mud layer. However, linkage with underlying banded intervals is inferred due to the common presence of fine carbonaceous material.

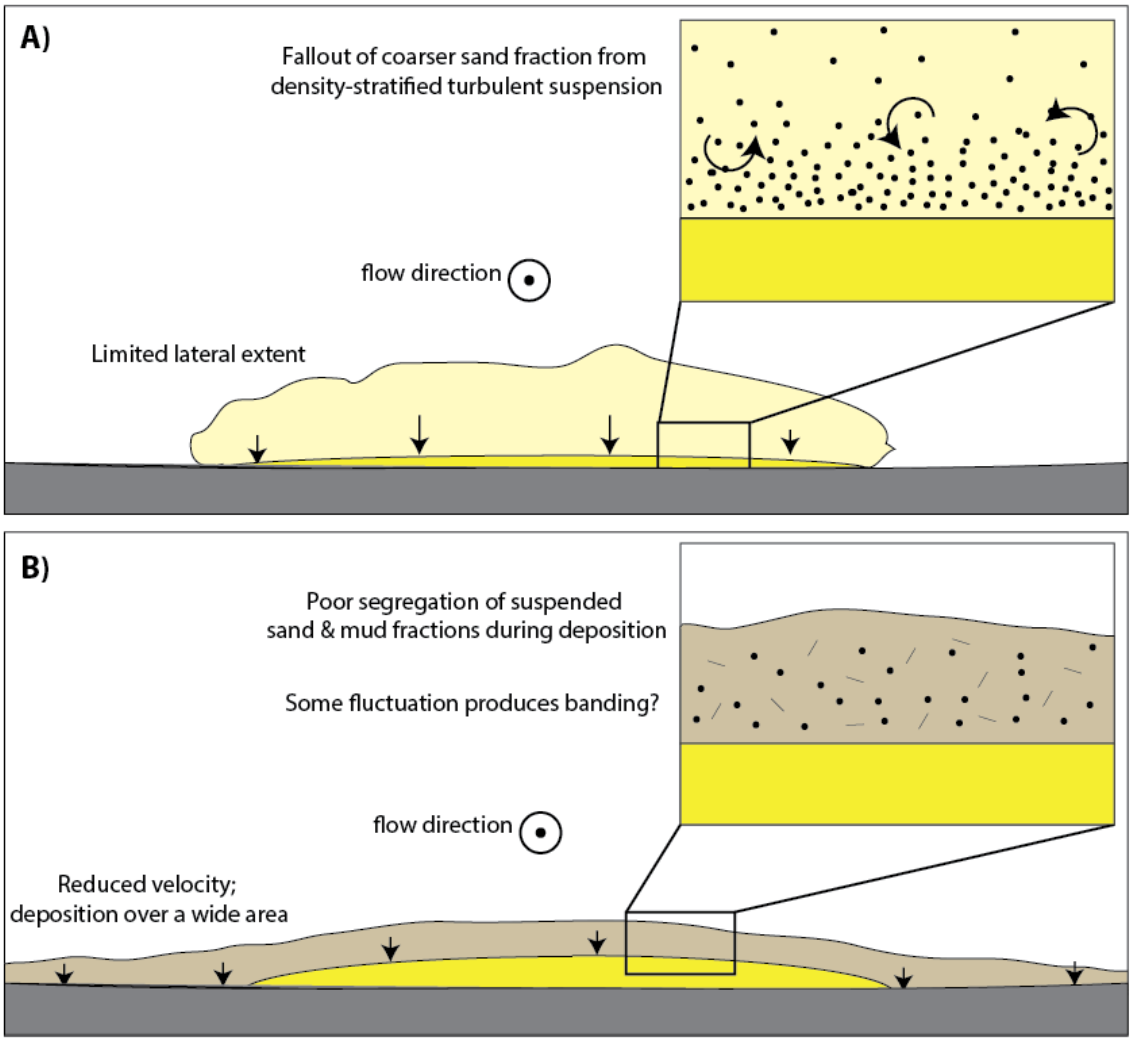

Figure 24. Graphic summary of depositional process models for (A) structureless sandstone divisions and (B) banded divisions.

6.4. Construction of TFD-dominated lobe architecture

The TFD-dominated lobe strata described here are shown to be internally complex and spatially heterogeneous. The evolution of individual transitional flows produces event beds in which coarser sandstone is restricted to bed axes and draped by extensive mud-rich deposits. An analogous internal architecture is observed for TFD-constructed lobe elements, where lateral pinch-out of structureless sandstones in stacked TFDs results in a dramatic change in net sand content from axis to margin. The vertical stacking of beds within lobe elements is proposed to reflect the focusing of flows along a common trajectory by a fixed up-dip feeder channel. Variability within lobe elements is therefore interpreted to primarily reflect differences between flows, such as variable flow volume and flow rheology, that result in differences between successive beds.

Fleming (2010) documented lateral offsets up to 1500 m between the axes of lobe elements in the Point Loma Formation. These offsets are interpreted to reflect compensational stacking of lobe elements, which causes the sand-prone axes of lobe elements to be more evenly distributed within lobe complexes. Straub and Pyles (2012) describe a similar pattern for the organization of architectural elements in lobe strata of the Carboniferous Ross Formation, in which compensation strength is observed to increase at larger hierarchical levels. Lateral shifts in location between lobe elements may reflect processes with larger spatial and temporal scales, such as feeder channel avulsion, which could be caused by a variety of allogenic and autogenic forcings (Prélat et al., 2010; Macdonald et al., 2010; Straub and Pyles, 2012).

6.5. Expression of lobe architecture in 1-D sections

A similar relationship between bimodal thickness frequency distributions and the presence of basal structureless sandstone divisions is observed for TFD-dominated strata in the Point Loma Formation. This might serve as further evidence that structureless sandstone divisions within turbidites and TFDs are generated by similar depositional processes. Lobe axis sections with abundant structureless sandstone intervals are fairly well described as a mixture of two lognormal distributions. This is interpreted to reflect: (1) a relative abundance of thick sandstone intervals resulting from a larger number of flows with trajectories along lobe axes, and; (2) alternation between sand-rich and mud-rich intervals that record lateral shifts in position between adjacent lobe elements.

Thinning and eventual pinch-out of structureless sandstone divisions results in a relatively narrow range of bed thicknesses and low variability toward the margin of the lower-central complex. This might suggest that bed thickness frequency distributions might be particularly well-suited for distinguishing relative axial versus marginal positions, while prior studies have emphasized bed thickness frequency distributions as potential indicators of relative proximal and distal environments (Carlson and Grotzinger, 2001; Sinclair and Cowie, 2003).

7: Conclusions

The combination of vertical and cross-flow exposure of individual TFDs in this outcrop provides insight into spatial and temporal changes in flow behavior. Additionally, high lateral continuity presents a unique opportunity to relate cross-flow variability within individual beds to larger-scale heterogeneity within lobe strata. Understanding the dimensions, internal variability, and spatial distribution of beds containing both coarser sand with relatively low mud content and mud-rich sand components is important for subsurface reservoir characterization. The spatial distribution of high-permeability and low-permeability layers within TFD-prone reservoirs is likely to significantly influence fluid flow. Furthermore, bed thickness frequency analysis shows how differences between distributions of vertically measured bed thicknesses relate to the observed spatial variability in outcrop. Developing a better understanding of these relationships is critical for a variety of applications in both industry and academia in which geoscientists are frequently limited to one-dimensional data sets. A summary of key conclusions from this study is provided below:

1) TFDs in the Point Loma Formation consistently show a bipartite internal structure where sandstone divisions undergo a shift in composition, fabric, and shape. Bed axes are sand-rich and structureless sandstones pinch out relatively quickly toward bed margins. Vertical and lateral transitions into mud-rich banded divisions are typically abrupt, and these divisions are laterally continuous at outcrop scale.

2) The common internal structure of TFDs is interpreted to reflect a reduction in the degree of mixing and hydraulic grain segregation between an initial density-stratified flow and a subsequent laterally extensive flow. Features of basal structureless sandstone intervals suggest that some flows were initially turbulent and deposited coarser sediment layer-by-layer. Structureless deposits with mud contents in excess of 25% are considered here as candidates for deposition from transitional flows; the high mud content in these divisions exceeds the maximum amount that be explained by trapping of fines during deposition of coarser sand. The transition to the overlying banded interval is interpreted to reflect a shift in flow rheology in which mixing and grain segregation are significantly inhibited, but interactions between cohesive fines are insufficient to induce wholesale transformation to debris flow.

3) Soft-sediment deformation is frequently observed in banded intervals and is most intense at bed axes. These features indicate liquefaction and isolated zones of fluidization within banded intervals that likely resulted from the combination of (1) rapid deposition of loosely-packed basal sand and (2) draping by low-permeability banded intervals. This relationship suggests that soft-sediment deformation may be characteristic for TFDs and similar deposits in other locations.

4) Turbidites and TFDs are present in proximal and distal lobe strata of the Point Loma Formation, but the relative abundance of each deposit type changes

dramatically from proximal to distal. TFDs with mud-rich sandstone divisions are found to dominate the exposed distal lobe strata, suggesting that most currents that transported sand to distal lobe environments contained large volumes of suspended mud. Although fine-grained material could have been incorporated as currents traversed muddy substrates between proximal and distal lobe settings, the scarcity of erosion surfaces and the absence of carbonaceous material in mud caps suggests that most of the mud fraction in TFDs originated further upstream. Another possibility is that currents were initially mud-rich at or near their upstream origins, and that flow transformation occurred in response to decreased lateral confinement and flow velocity in distal lobe environments.

5) Cross-flow variability within TFD-dominated lobe strata is shown to result from the combination of (1) vertical stacking of individual TFDs to from lobe elements and (2) compensational stacking of lobe elements at larger spatial and temporal scales. This combination reflects a transition from spatial variability that is dominated by the dynamics of depositing currents at the bed and lobe element scales to variability that is increasingly influenced by larger-scale processes at higher hierarchical levels.

6) Comparison of frequency distributions for bed thicknesses from vertical sections may be useful for distinguishing different lobe environments. Bimodality is observed to be strongly associated with lobe axes, regardless of the relative proximal or distal environment. Aside from an overall decrease in bed thicknesses

from proximal to distal, the thickness distributions for turbidite-dominated and TFD-dominated strata at lobe axes appear fairy similar. The absence of bimodality in bed thickness distributions from off-axis and lobe margin sections reflects the pinch out of structureless sandstone divisions toward lobe margins. This suggests that bed thickness frequency distributions might be particularly useful for distinguishing between axial and marginal lobe environments.

Appendices

Appendix A: Section locations and summary information

Section ID	Field Region	Latitude	Longitude	Total Thickness (cm)	Beds
011 (F)	Central	32.699971	-117.255124	500.0	52
012	South	32.673954	-117.245524	97.0	7
015	South	32.672891	-117.245391	94.0	7
016	South	32.672649	-117.245454	85.0	7
017	South	32.673461	-117.245350	84.0	7
018 (G)	South	32.674319	-117.245753	768.7	73
019	South	32.672141	-117.245542	90.0	8
020	South	32.672025	-117.245402	91.0	10
021	South	32.671745	-117.245385	83.0	9
044 (D)	Central	32.712267	-117.256043	909.2	217
045 (B)	North	32.719929	-117.257191	668.5	52
046 (D)	Central	32.713656	-117.256345	749.0	58
049 (A)	North	32.721540	-117.257230	732.5	35
050	North	32.725277	-117.258305	70.0	4
051 (C)	North	32.716016	-117.255696	465.6	67
052 (E)	Central	32.706978	-117.255562	767.6	118
053	Central	32.696058	-117.253719	76.5	4

Table 3. Locations, total thicknesses, and number of beds for all measured sections.

Appendix B: Interval thickness data

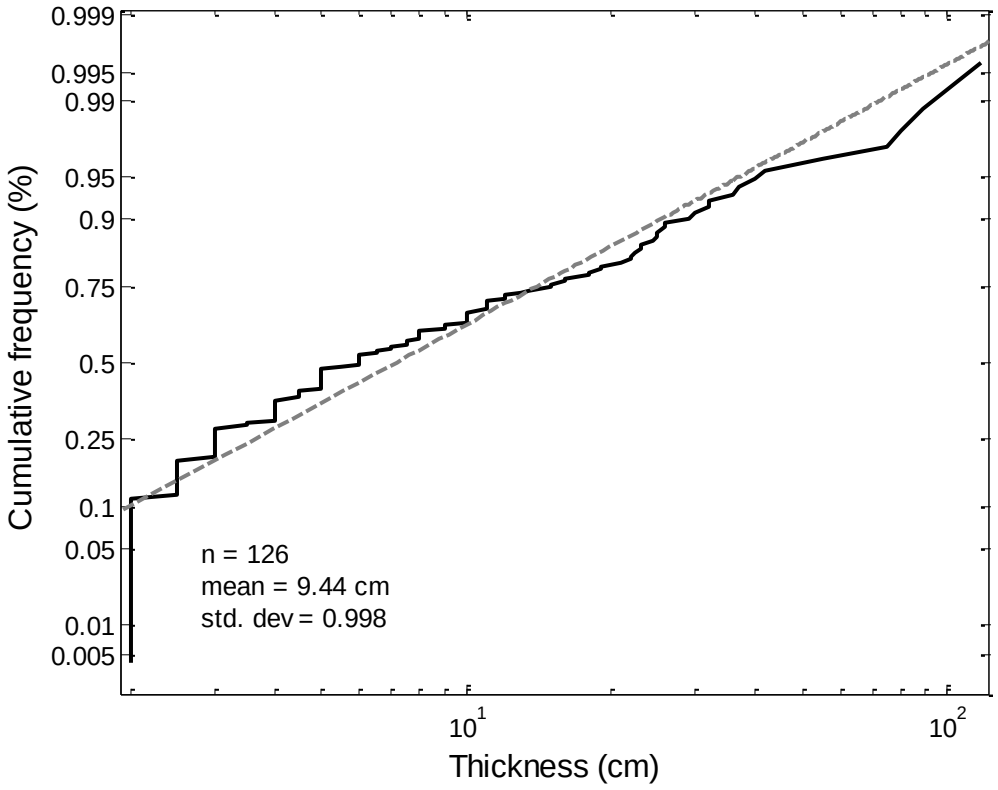

Figure 25. Cumulative probability plot of thickness data and lognormal distribution fit (dashed curve) for 126 structureless sandstones in the Point Loma Formation. Mean refers to the geometric mean and std. dev. is the standard deviation of the log-transformed thickness data.

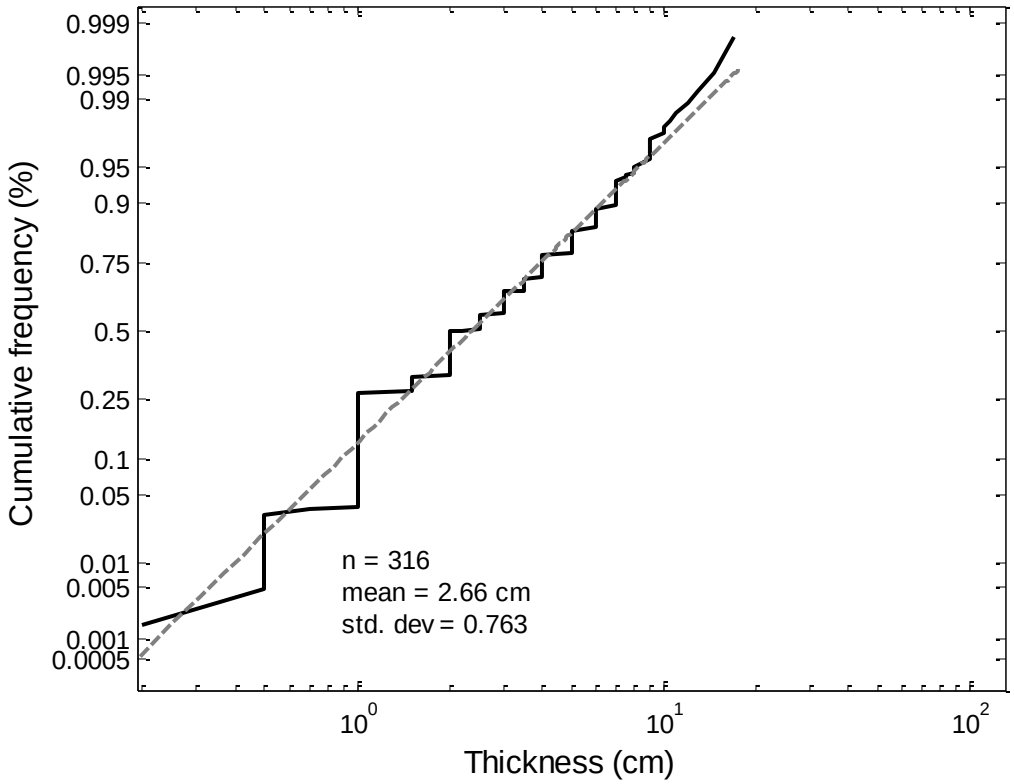

Figure 26. Cumulative probability plot of thickness data and lognormal distribution fit (dashed curve) for 316 banded sandstones in the Point Loma Formation. Mean refers to the geometric mean and std. dev. is the standard deviation of the log-transformed thickness data.

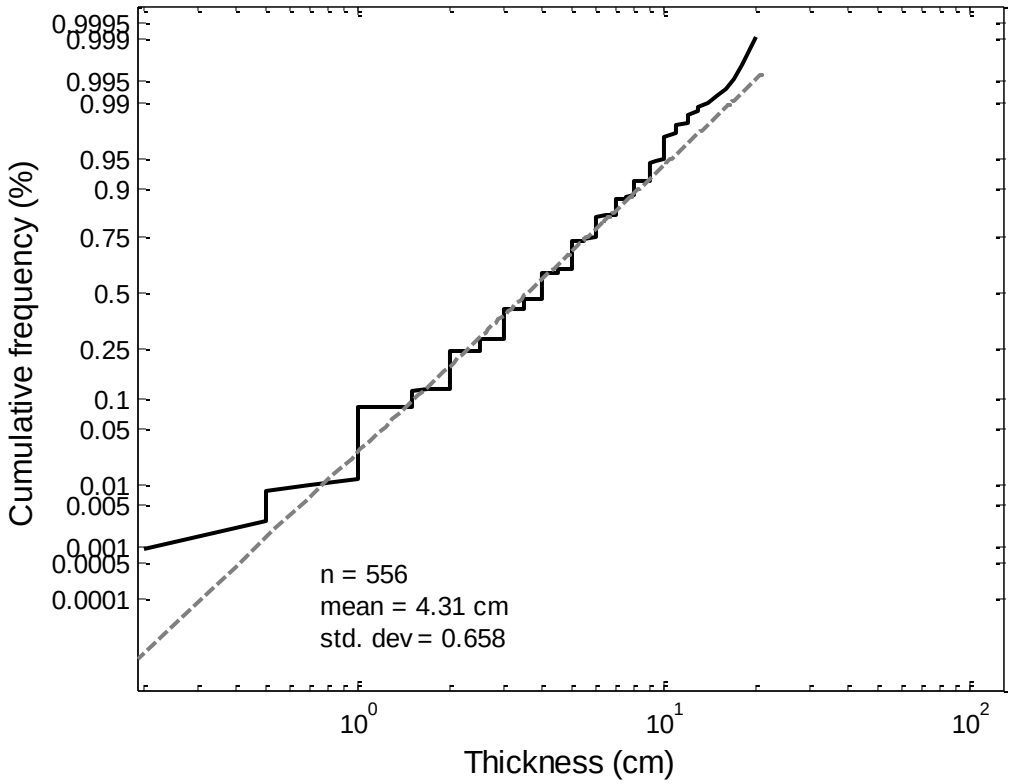

Figure 27. Cumulative probability plot of thickness data and lognormal distribution fit (dashed curve) for 556 mudstones in the Point Loma Formation. Mean refers to the geometric mean and std. dev. is the standard deviation of the log-transformed thickness data.

Appendix C: Grain size sample locations and measurement data

Sample ID	Loc. ID	Field Region	Facies	Mud %	Modal grain size (μm)	Dx 10	Dx 50	Dx 90	Facies Thickness (cm)
PL-001	044	Central	StS	21.2	200	20.29	168.86	325.96	21
PL-002	044	Central	StS	24.3	270	19.15	185.24	476.91	23
PL-020	011	South	StS	30.3	135	10.00	116.47	236.27	50
A04_B	015	South	StS	28.9	126	13.79	110.28	215.25	25
A05_B	017	South	StS	34.6	111	18.49	101.36	202.06	27
A06-B	012	South	StS	18.2	135	34.64	136.56	292.47	28.5
A07-B	018	South	StS	23.6	120	20.93	119.68	381.20	23
A08_B	019	South	StS	29.5	160	15.11	127.99	258.38	13
A09_B	020	South	StS	30.8	105	16.91	95.02	183.13	12
PL-021	011	South	StS	28.9	140	14.66	114.84	232.55	19
PL-023	011	South	StS	21.1	113	20.78	108.96	195.33	13
PL-024	049	North	StS	23.1	255	22.27	187.02	470.60	118
PL-025	049	North	StS	39.5	211	5.29	121.77	288.87	37
PL-026	049	North	StS	17.2	310	19.97	267.29	720.93	42
PL-027	049	North	StS	21.3	375	14.15	268.30	710.54	25
PL3-04	053	Central	StS	33.9	280	4.94	137.67	410.70	16
PL-011	046	Central	StS	36.6	255	5.77	131.42	388.03	19
PL3-01	045	North	StS	38.7	150	3.98	97.61	236.03	15
PL3-02	045	North	Bnd	57.5	111	4.61	57.67	203.08	20
PL3-05	053	Central	Bnd	46.0	111	4.53	85.13	239.54	5
PL3-07	053	Central	Bnd	65.9	90	2.06	48.66	128.79	7
A10_B	021	South	Bnd	27.4	105	10.57	79.97	199.83	4
A04_D	015	South	Bnd	29.1	111	19.59	100.45	200.76	12
A05_D	017	South	Bnd	50.8	98	9.47	74.43	184.04	13
A06_D	012	South	Bnd	44.7	71	9.45	75.70	310.96	9
A07_D	018	South	Bnd	32.3	109	10.78	104.32	289.70	11
A08_D	019	South	Bnd	67.3	72	5.42	39.45	125.75	7
A10_D	021	South	Bnd	64.2	95	3.73	35.88	149.15	8

Table 4. Sampling locations, grain size measurement data, facies and thicknesses for all laboratory-measured samples. StS refers to the structureless sandstone facies and Bnd is banded sandstone.

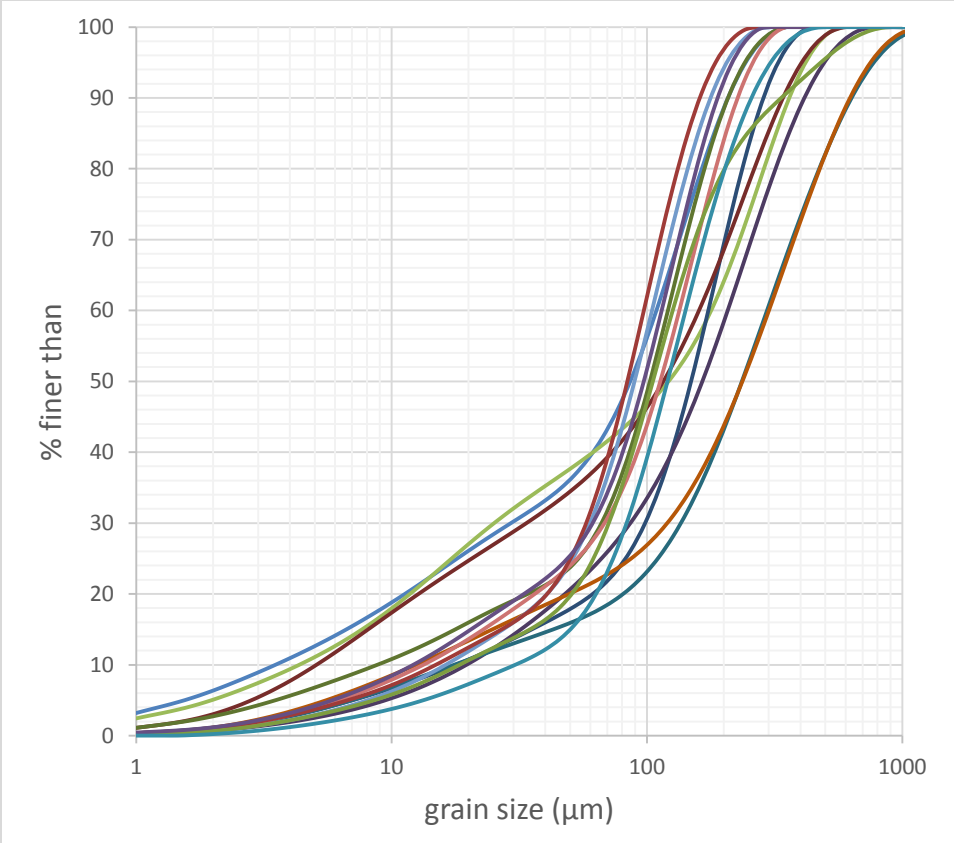

Figure 28. Cumulative probability plot of structureless sandstone grain size data for laboratory-measured samples. Grain size variability between most samples appears to occur primarily between the upper ~75-80% of each distribution.

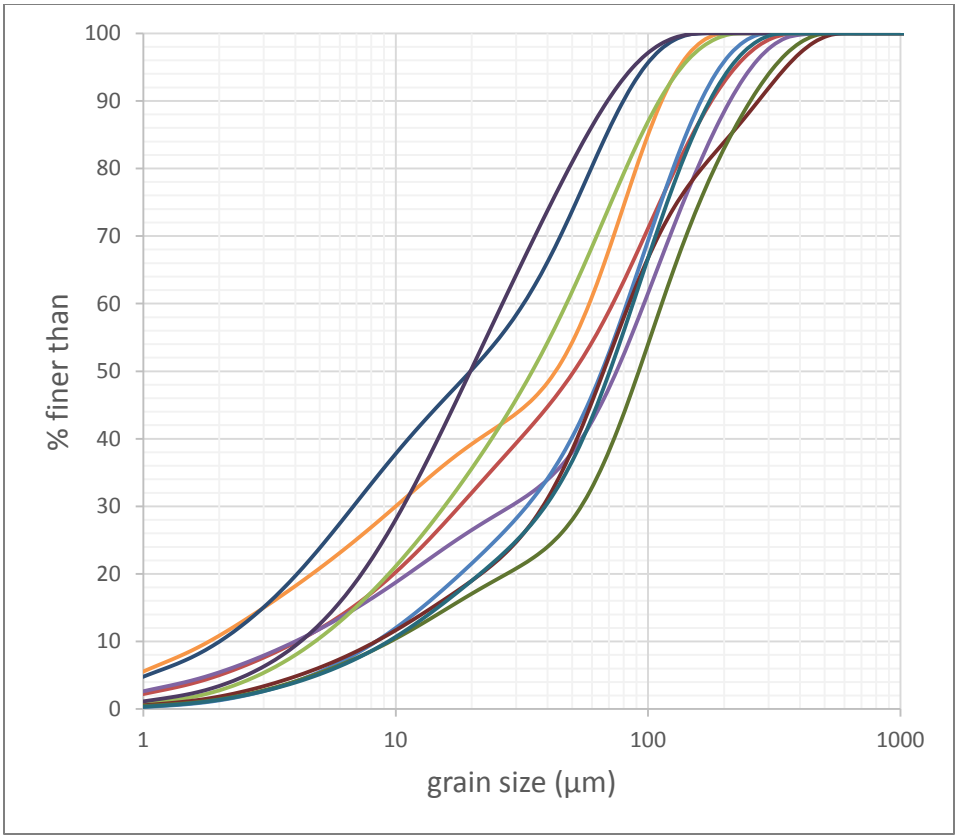

Figure 29. Cumulative probability plot of grain size data for laboratory-measured samples of the banded facies.

Appendix D: Maximum thicknesses and thinning rates for TFD divisions

Bed ID	Facies	Maximum thickness (cm)	Thinning rate
S1	StS	27	0.0015
S3	StS	12	0.0012
IM-1	StS	105	0.0022
G44-1	StS	12	0.0267
G44-2	StS	14	0.0140
S4	StS	20	0.0011
S5	StS	17	0.0034
c1-1	StS	23	0.0067
c2-1	StS	17	0.0020
S1	Bnd	13	0.0004
S2	Bnd	5	0.0002
S3	Bnd	5	0.0002
IM-1	Bnd	10	0.0004
S5	Bnd	5	0.0003
CB-1	Bnd	4	0.0002
CB-2	Bnd	3	0.0002

Table 5. Table of data presented in Figure 10. Table values include maximum thicknesses measured at bed axes and axis-to-margin thinning rates. StS refers to the structureless sandstone facies and Bnd is banded sandstone.

References

Allen, J.R.L., 1977, The possible mechanics of convolute lamination in graded sand beds, Journal of the Geological Society of London, 134, 19-31.

Allen, J.R.L., 1982, Chapter 10, Structures and sequences related to gravity-current surges, In: Sedimentary Structures. Their Character and Physical Basis, Elsevier, Amsterdam, 395–431.

Amy, L.A, and Talling, P.J., 2006, Anatomy of turbidites and linked debrites based on long distance (120 x 30 km) bed correlation, Marnoso Arenacea Formation, Northern Apennines, Italy. Sedimentology, 53, 161-212.

Arnott, R.W.C. and Hand, B.M., 1989, Bedforms, primary structures and grain fabric in the presence of suspended sediment rain, Journal of Sedimentary Petrology. 59, 1062–1069.

Atwater, T., 1970, Implications of plate tectonics for the Cenozoic tectonic evolution of western North America: Geological Society of America Bulletin. 81, 3513-3536.

Bannerjee, I., 1977, Experimental study on the effect of deceleration on the vertical sequence of sedimentary structures in silty sediments. Journal of Sedimentary Petrology, 47, 771–783.

Barker, S.P., Haughton, P.D.W., McCaffrey, W.D., Archer, S.G., Hakes, B., 2008. Development of rheological heterogeneity in clay-rich high-density turbidity currents: Aptian Britannia Sandstone Member, U.K. Continental shelf. Journal of Sedimentary Research 78, 45–68.

Best, J. and Bridge, J., 1992, The morphology and dynamics of low amplitude bedwaves upon upper stage plane beds and the preservation of planar laminae. Sedimentology, 39, 737–752.

Bouma, A.H., 1962, Sedimentology of some flysch deposits: A graphic approach to facies interpretation. Amsterdam, Elsevier, 48-51, 98-99.

Carlson, J. and Grotzinger, J. P., 2001, Submarine fan environment inferred from turbidite thickness distributions. Sedimentology, 48, 1331–1351.

Carter, R.M., 1975, A discussion and classification of subaqueous mass-transport with particular application to grain-flow, slurry-flow and fluxoturbidites. Earth Science Reviews, 11, 145-177.

Dempster, A.P., Laird, N.M. and Rubin, D.B., 1977, Maximum likelihood from incomplete data via the EM algorithm. Journal of the Royal Statistical Society: Series B, 39, 1–22.

Fleming, A., 2010, Stratigraphic architecture of lobe strata in a submarine fan setting, Point Loma Formation, California (Unpublished master's thesis). Colorado School of Mines, Golden, Colorado, USA, 133 p.

Flemings, P.B., Long, H., Dugan, B., Germaine, J., John, C.M., Behrmann, J.H., Sawyer, D., 2008. Pore pressure penetrometers document high overpressure near the seafloor where multiple submarine landslides have occurred on the continental slope, offshore Louisiana, Gulf of Mexico. Earth and Planetary Science Letters 269, 309-325.

Haughton, P.D.W., Barker, S.P., and McCaffrey, W.D., 2003, "Linked" debrites in sand-rich turbidite systems—origin and significance: Sedimentology, 50, 459-482.

Haughton, P., Davis, C., McCaffrey, W., and S. Barker, 2009, Hybrid sediment gravity flow deposits – Classification, origin and significance: Marine and Petroleum Geology, 26, 1900-1918.

Hirayama, J. and Nakajima, T., 1977, Analytical study of turbidites, Otadai Formation, Boso Peninsula, Japan. Sedimentology, 24, 747–779.

Hodgson, D.M., 2009, Distribution and origin of hybrid bed sin sand-rich submarine fans of the Tanqua depocentre, Karoo Basin, South Africa: Marine and Petroleum Geology, 26, 1940-1956.

Ito, M., 2008, Downfan transformation from turbidity currents to debris flows at a channel-to-lobe transitional zone: the lower Pleistocene Otadai Formation, Boso Peninsula, Japan. Journal of Sedimentary Research 78, 668–682.

Jones, S.D., and Peterson, G.L., 1973, Provenance of the Upper Cretaceous Cabrillo Formation at Point Loma and La Jolla, California in Ross, A., Dowlen, R.J., eds., Studies on the geology and geological hazards of the greater San Diego California: San Diego Association, Geologists field trip guidebook, 23-25.

Kane, I.A. and A. Ponten, 2012, Submarine transitional flow deposits in the Paleogene Gulf of Mexico: Geology, 40, 1119-1122.

Kennedy, M.P., and Moore, G.W., 1971, Stratigraphic relations of upper Cretaceous and Eocene Formation, San Diego coastal area, California: The American Association of Petroleum Geologists Bulletin, 55, 709-722.

Kennedy, M.P., and Tan, Siang, S.S., 2005, Geologic map of the San Diego 30'x60' quadrangle, California: USGS, Regional Geological Map Series, 1:100,000 Scale, Map n. 3, 2 p.

Kennedy, M.P., 1975, Western San Diego metropolitan area: Del Mar, La Jolla, and Point Loma 7.5 minute quadrangles in Geology of the San Diego metropolitan area, California, Bulletin 200, 9-38.

Kneller, B.C. and Branney, M.J., 1995, Sustained high-density turbidity currents and the deposition of thick massive sands. Sedimentology, 42, 607–616.

Kneller, B. C., & McCaffrey, W. D., 2003, The interpretation of vertical sequences in turbidite beds: the influence of longitudinal flow structure. Journal of Sedimentary Research, 73, 706-713.

Kuenen, P.H.,1966, Experimental turbidite lamination in a circular flume. The Journal of Geology, 74, 523–545.

Leclair, S.F. and Arnott, R.W.C., 2005, Parallel lamination formed by high-density turbidity currents. Journal of Sedimentary Research, 75, 1–5.

Leeder, M.R., Alexander, J., 1987, The origin and tectonic significance of asymmetrical meander belts. Sedimentology, 34, 217–226.

Lilliefors, H.W., 1967, On the Kolmogorov-Smirnov test for normality with mean and variance unknown, Journal of the American Statistical Association, 62, 399-402

Lowe, D.R., Guy, M., 2000, Slurry-flow deposits in the Britannia Formation (lower Cretaceous), North Sea: a new perspective on the turbidity current and debris flow problem: Sedimentology, 47, 31-70.

Lowe, D.R., 1979, Sediment gravity flows: their classification and some problems of application to natural flows and deposits: Society of Economic Paleontologists and Mineralogists Special Publication 27, 75-82.

Lowe, D.R., 1982, Sediment gravity flows II: depositional models with special reference to the deposits of high-density turbidity currents: Journal of Sedimentary Petrology, 52, 278-297.

Lyons, W.J., Quantifying Channelized Submarine Depositional Systems from Bed to Basin Scale (Unpublished doctoral dissertation). Massachusetts Institute of Technology, Cambridge, Massachusetts, USA, 139-170.

Macdonald, H.A., Wynn, R.B., Huvenne, V.A.I., Peakall, J., Masson, D.G., Weaver, P.P.E. and McPhail, S.D., 2011, New insights into the morphology, fill, and

remarkable longevity (>0.2 m.y.) of modern deep-water erosional scours along the northeast Atlantic margin. Geosphere, 7, 845–867.

Maltman, A. J., and A. Bolton, 2003, How sediments become mobilized, in P. van Rensbergen, R. R. Hillis, A. J. Maltman, and C. K. Morley, eds., Subsurface sediment mobilization: Geological Society (London) Special Publication 216, 9–20.

Middleton, G. V., and Hampton, M. A., 1976, Subaqueous sediment transport and deposition by sediment gravity flows, in Stanley, D. J., and Swift, D. J. P., eds., Marine Sediment Transport and Environmental Management: New York, Wiley, 197-218.

Moretti, M., 2000, Soft-sediment deformation structures interpreted as seismites in middle-late Pleistocene aeolian deposits (Apulian foreland, southern Italy). Sedimentary Geology, 135, 167–179.

Moretti, M., Soria, J.M., Alfaro, P., Walsh, N., 2001, Asymmetrical soft-sediment deformation structures triggered by rapid sedimentation in turbiditic deposits (Late Miocene, Guadix Basin, Southern Spain). Facies, 44, 283–294.

Murray, C.J., Lowe, D.R., Graham, S.A., Martinez, P.A., Zeng, J., Carroll, A., Cox, R., Hendrix, M., Heubeck, C., Miller, D., Moxon, I.W., Sobel, E., Wendebourg, J. and Williams, T., 1996, Statistical analysis of bed-thickness patterns in a turbidite section from the Great Valley Sequence, Cache Creek California. Journal of Sedimentary Petrology, 66, 900–908.

Mutti, E., 1992, Turbidite sandstones: Agip. San Donato Milanese, Parma, Italy, 236 p.

Nardin, T.R., Hein, F.J., Gorsline, D.S. and Edwards, B.D., 1979, A review of mass movement processes, sediment and acoustic characteristics, and contrasts in slope and baseofslope systems versus canyon-fan-basin floor systems. In: Geology of Continental Slopes (Eds L.J. Doyle and O.H. Pilkey), SEPM Special Publication, 27, 61–73.

Nichols, R.J., 1995, The liquefaction and remobilization of sandy sediments. In: *Characterization of Deep Marine Clastic Systems* (Eds A.J. Hartley and D.J. Prosser), *Geological Society of London, Special Publication*, 94, 63–76.

Nilson, T.H., and Abbott, P.L., 1979, Turbidite sedimentology of the upper Cretaceous Point Loma and Cabrillo Formations, in Abbott, P.L., ed., Geological excursions in the southern California area: San Diego State University Department of Geological Science, 139-166.

Nilson, T.H., and Abbott, P.L., 1981, Paleogeography and sedimentology of upper Cretaceous turbidites, San Diego, California. The American Association of Petroleum Geologists, 1256-1270.

Obermeier, S.F., 1996, Use of liquefaction-induced features for paleoseismic analysis—an overview of how liquefaction features can be distinguished from other features and how their distribution and properties of source sediment can be used to infer the location and strength of Holocene paleo-earthquakes. Engineering Geology, 44, 1–76.

Owen, G., Moretti, M. and Alfaro, P. (Eds), 2011, Recognising triggers for soft-sediment deformation: current understanding and future directions. Sedimentary Geology, 235, 3/4.

Owen, G., 1987, Deformation processes in unconsolidated sands. In: Jones, M.E., Preston, R.M.F. (Eds.). Deformation of Sediments and Sedimentary Rocks, Geological Society Special Publication, 29, 11–24.

Owen, G., 1996, Experimental soft-sediment deformation: structures formed by the liquefaction of unconsolidated sands and some ancient examples. Sedimentology 43, 279–293.

Peterson, G.L., 1970, Distinction between Cretaceous and Eocene conglomerate in the San Diego area, southwestern California in Pacific slope geology of northern Baja California and adjacent Alta California: American Association of Petroleum Geologists, Pacific Section Field Trip Guidebook, 90-98.

Pickering, K., Stow, D. A. V., Watson, M., and Hiscott, R., 1986, Deep-water facies, processes and models: a review and classification scheme for modern and ancient sediments. Earth-Science Reviews, 23, 75–174.

Prélat, A., Covault, J.A., Hodgson, D.M., Fildani, A., and Flint, S.S., 2010, Intrinsic controls on the range of volumes, morphologies, and dimensions of submarine lobes: Sedimentary Geology, v. 232, 66–76

Pyles, D.R., 2007, Architectural elements in a ponded submarine fan, Carboniferous Ross Sandstone, Western Ireland in Nilson, T.H., Shew, R.D., Steffens, G.S., Studlick, J.R.J., eds., Atlas of deepwater outcrops: American Association of Petroleum Geologist Studies in Geology 56, CD-ROM, p 1-19.

Sadler, P., 1982, Bed-thickness and grain size of turbidites. Sedimentology, 29, 37–51.

Shanmugam, G., 1996, High-density turbidity currents: are they sandy debris flows? Journal of Sedimentary Research, 66, 2–10.

Shiki, T., Kumon, F., Inouchi, Y., Kontani, Y., Sakamoto, T., Tateishi, M., Matsubara, H., Fukuyama, K., 2000, Sedimentary features of the seismo-turbidites, Lake Biwa, Japan. Sedimentary Geology 135 (1–4), 37 – 50.

Sims, J.D., 1973, Earthquake-induced structures in sediments of Van Norman Lake, San Fernando, California. Science 182, 161–163.

Sinclair, H.D. and P.A. Cowie, 2003, Basin-floor topography and the scaling of turbidites. The Journal of Geology 11, 277-299

Silter, W.V., 1979, Cretaceous foraminifers from La Jolla, California in Geological excursions in the Southern California area (Abbott, P.L. eds), Department of Geological Services: San Diego University, San Diego, 171-172.

Stammer, J.G., 2014, Hydrodynamic fractionation of minerals and textures in submarine fans: Quantitative analysis from outcrop, experimental, and subsurface studies (Unpublished doctoral dissertation). Colorado School of Mines, Golden, Colorado, USA, 186 p.

Stevenson, C.J., Talling, P.J., Masson, D.G., Sumner, E.J., Frenz, M. and Wynn, R.B., 2014, The spatial and temporal distribution of grain-size breaks in turbidites. Sedimentology, 61, 1120-1156.

Straub, K. and D. R. Pyles, 2012, Quantifying the hierarchical organization of compensation in submarine fans using surface statistics: Journal of Sedimentary Research, v. 82, p. 889- 898.

Sumner, E.J., Amy, L. and Talling, P.J., 2008, Deposit structure and processes of sand deposition from a decelerating sediment suspension. Journal of Sedimentary Research, 78, 529–547.

Sylvester, Z. and Lowe, D.R., 2004, Textural trends in turbidites and slurry beds from the Oligocene flysch of the East Carpathians, Romania. Sedimentology, 51, 945–972.

Sylvester, Z., 2007, Turbidite bed thickness distributions: methods and pitfalls of analysis and modelling. Sedimentology, 54, 847–870.

Talling, P.J., Amy, L.A. Wynn, R.B, Peakall, J., and Robinson, M., 2004, Beds comprising debrite sandwiched within co-genetic turbidite: origin and widespread occurrence in distal depositional environments: Sedimentology, 51, 163-194.

Talling, P.J., Malgesini, G. and Felletti, F., 2012a, Can liquefied (debris) flows deposit clean sandstone over large areas of sea floor? Field evidence from the Marnoso-arenacea Formation, Italian Apennines. Sedimentology, doi: 10.1111/ j.1365-3091.2012.01358.x.

Talling, P., J., Masson, D.G., Sumner, E.J., and G. Malgesini, 2012b, Subaqueous sediment density flows: Depositional processes and deposit types: Sedimentology, v. 59, 1937- 2003.

Talling, P.J., 2001, On the frequency distribution of turbidite thickness. Sedimentology, 48, 1297–1331.

Tsui, P.C., 2006, EM algorithm for k multidimensional Gaussian mixture estimation (http://www.mathworks.com/matlabcentral/fileexchange/9659-fast-em-gm), MATLAB Central File Exchange. Retrieved November 12, 2014.

Vrolijk, P.J. and Southard, J.B., 1997, Experiments on rapid deposition of sand from high-velocity flows. Geoscience Canada, 24, 45–54.

Yeo, R.K., 1982, The stratigraphy and sedimentology of upper Cretaceous sediments of southwestern California and Baja California, Mexico: Unpublished PhD Thesis, Rice University.

Yeo, R.K., 1984, Miocene and Cretaceous depositional environments northwestern Baja California, Mexico: Annual Meeting Pacific Section American Association of Petroleum Geologist, San Diego, California, April 18-21, 57-68.